AD-A048 465 DYNAMICS TECHNOLOGY INC TORRANCE CALIF* F/G 20/4
AN ANALYTICAL STUDY OF THE EFFECT OF SURFACE ROUGHNESS ON BOUND--ETC(U)
OCT 77 C L MERKLE, K T TZOU, T KUBOTA N00014-77-C-0005
UNCLASSIFIED DT-7606-4 NL

1 OF 1
AD A048465

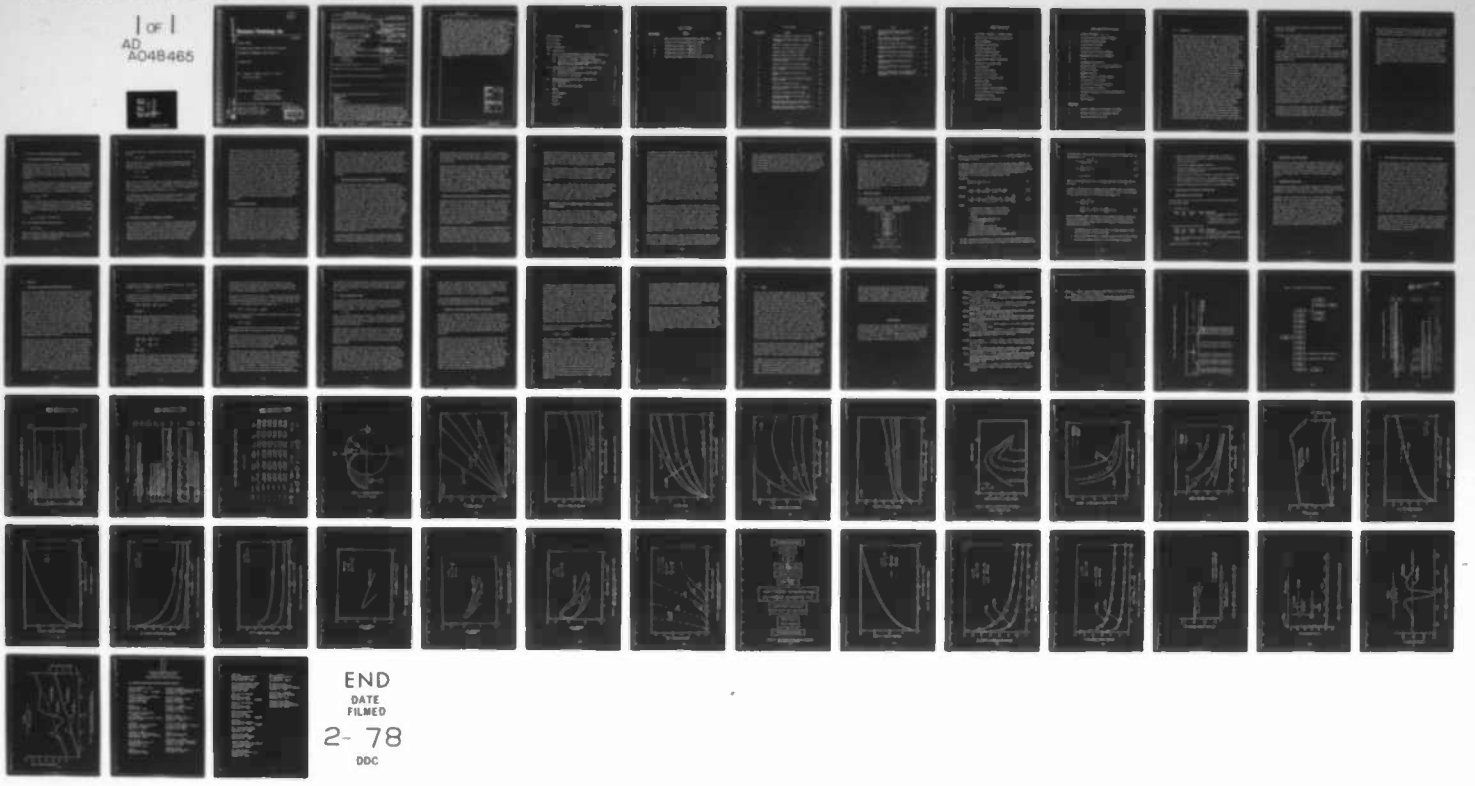

END
DATE FILMED
2-78
DDC

(12 b.s.)

Dynamics Technology, Inc.

DT-7606-4

FINAL REPORT

AN ANALYTICAL STUDY OF THE EFFECT OF SURFACE ROUGHNESS ON BOUNDARY-LAYER STABILITY

OCTOBER 1977

BY: CHARLES L. MERKLE, KENT T. S. TZOU,
AND TOSHI KUBOTA

SUPPORTED BY: DEFENSE ADVANCED RESEARCH
PROJECTS AGENCY AND
OFFICE OF NAVAL RESEARCH
CONTRACT N00014-77-C-0005

DYNAMICS TECHNOLOGY, INC.
3838 CARSON STREET, SUITE 110
TORRANCE, CALIFORNIA 90503

UNCLASSIFIED

SECURITY CLASSIFICATION OF THIS PAGE (When Data Entered)

REPORT DOCUMENTATION PAGE

READ INSTRUCTIONS BEFORE COMPLETING FORM

1. REPORT NUMBER

2. GOVT ACCESSION NO.

3. RECIPIENT'S CATALOG NUMBER

4. TITLE (and Subtitle)
An Analytical Study of the Effect of Surface Roughness on Boundary-Layer Stability.

5. TYPE OF REPORT & PERIOD COVERED
Final Report.
29 Nov 76 - 30 Sept 77

6. PERFORMING ORG. REPORT NUMBER
DT-7606-4

7. AUTHOR(s)
Charles L. Merkle, Kent T. S. Tzou
Toshi Kubota

8. CONTRACT OR GRANT NUMBER(s)
Contract N00014-77-C-0005

9. PERFORMING ORGANIZATION NAME AND ADDRESS
Dynamics Technology, Inc.
3838 Carson Street, Suite 110
Torrance, California 90503

10. PROGRAM ELEMENT, PROJECT, TASK AREA & WORK UNIT NUMBERS

11. CONTROLLING OFFICE NAME AND ADDRESS
Office of Naval Research, Department of the Navy
800 North Quincy Street
Arlington, Virginia 22217

12. REPORT DATE
October 1977

13. NUMBER OF PAGES
66

14. MONITORING AGENCY NAME & ADDRESS(if different from Controlling Office)
69p.

15. SECURITY CLASS. (of this report)
Unclassified

15a. DECLASSIFICATION/DOWNGRADING SCHEDULE

16. DISTRIBUTION STATEMENT (of this Report)

Approved for public release; distribution unlimited.

17. DISTRIBUTION STATEMENT (of the abstract entered in Block 20, if different from Report)

18. SUPPLEMENTARY NOTES

19. KEY WORDS (Continue on reverse side if necessary and identify by block number)
Boundary layer
Heating
Stability
Surface roughness
Transition

20. ABSTRACT (Continue on reverse side if necessary and identify by block number)

The effects of surface roughness on the transition of a laminar boundary layer are basically two-fold: i) it can distort the mean velocity and temperature profiles thus altering the stability characteristics of the layer and ii) it can induce additional disturbances to the boundary layer which may lead to an earlier transition. Only the first of these effects is considered in this report. Three different types of surface roughness are investigated here; distributed roughness, surface waviness, and a single two-dimensional bump. An analytical model which describes the effect of distributed roughness on the mean flow and its stability

DD FORM 1473 (FACSIMILE)

SN 393 137

UNCLASSIFIED

SECURITY CLASSIFICATION OF THIS PAGE (When Data Entered)

is described. This model is further validated by comparison with Achenbach's experimental results and is then applied to the flow about an underwater body in order to illustrate the effects of surface roughness in a more realistic situation. It is found that surface heating in the presence of surface roughness is far less effective at prolonging laminar flow than for the smooth wall situation. The incorporation of this model into the existing TAPS code is also described. For surface waviness (resulting from manufacturing, perhaps), Lessen's model is extended here to provide a qualitative assessment of its effect. The preliminary results suggest a weak effect for expected surface waviness characteristics. The third type of surface irregularity - a single two-dimensional bump - is addressed using Smith's triple-deck formulation. Preliminary analysis is presented to provide the foundation for a future quantitative assessment of the effects of surface roughness of this type, if needed. In summary, surface irregularities can play a dominant role in determining the practical limit for the application of boundary-layer control techniques. The present distributed roughness model as incorporated into the TAPS code can provide a reasonable prediction of its effect in the presence of boundary-layer control techniques (shaping, heating, suction) on the transition location for an underwater vehicle. As a final caution, extreme care should be taken in the interpretation of any experimental results, if no quantitative surface finish information is known.

TABLE OF CONTENTS

LIST OF TABLES

LIST OF FIGURES

SYMBOLS AND NOTATION

A^+	"Van Driest" parameter in roughness model
C_p	Specific heat; also, pressure coefficient
G	Görtler parameter
h	Amplitude of surface wave
H	Enthalpy; shape factor
k	Effective roughness height
K	Laminar thermal conductivity
K_T	Total/effective thermal conductivity
K_ε, K'_ε	Parameters in roughness model
p	Static pressure
Pr	Laminar Prandtl number
Pr_t	Turbulent Prandtl number
r_o	Radius of an axisymmetric body
Re	Reynolds number
T	Static temperature
u	Local streamwise velocity component
v	Local normal velocity component
x	Streamwise coordinate
y	Coordinate normal to surface

α	Complex wave number = $\alpha_r + i\,\alpha_i$
β	Falkner-Skan pressure gradient parameter
β_1	Parameter in roughness model
δ	Boundary-layer thickness
δ^*	Displacement thickness
ε_H	Thermal diffusivity due to roughness
ε_M	Momentum diffusivity due to roughness
ΔT	$T - T_e$
λ^*	Wavelength of surface wave
η	Normal coordinate in Levy-Lees transformation
ζ	Radius of curvature
θ	Momentum thickness
Φ	Angular location on cylinder, degrees
μ	Laminar molecular viscosity
μ_T	Total/effective molecular viscosity
ν	Laminar kinematic viscosity
ξ	Streamwise coordinate in Levy-Lees transformation
ρ	Density
ω	Real frequency

Subscripts

e	Quantity evaluated at the boundary-layer edge
k	Quantity evaluated at the roughness height
w	Quantity evaluated at the wall

1.0 INTRODUCTION

Recent technical advances have successfully demonstrated the feasibility of maintaining a laminar boundary layer over the surface of an underwater body operating at a moderately high Reynolds number (or speed). Various means of boundary-layer control techniques which allow this capability to be extended to substantially higher Reynolds numbers have been developed and tested, or are being tested, both in small-scale laboratory and in field experiments. The current techniques for delaying the onset of boundary-layer transition which, moveover, reduce the total viscous drag at high Reynolds number include body shaping, surface heating and suction through the surface. Depending on the specific application, one or a combination of these techniques can be used. The design of such low-drag, advanced, underwater vehicles relies critically on the ability to predict quantitatively the various phenomena which might affect the transition location. For years, the most successful schemes for predicting the location of boundary-layer transition have either relied on empirical data correlations (which work well for a restricted range of parameters) or on the semi-empirical "e^n" criterion (which is based on a coupling of linear stability calculations and empirical results). Both methods suffer from empiricism which restricts their validity to a limited parameter domain. The "e^n" method, in particular, has been considered as adequate for estimating the transition location on a smooth surface over the range of parameters for which data exist. The validation of the "e^n" method for higher Reynolds number flows using various boundary-layer control techniques has not been conclusive. Various investigations, both analytical and experimental, are underway to provide a more reliable means of predicting the location of boundary-layer transition. At the present time, the engineering design tool most commonly used is the TAPS program (Transition Analysis Program System) developed by McDonnell Douglas (Gentry, 1976). This computer program does not include the effects of several potentially important factors which are present in a realistic environment, however. For example, the effects of freestream disturbances (either acoustic waves or turbulence) and surface roughness, (either distributed or isolated) have not been incorporated into TAPS despite the fact that they, conceivably, could be the dominant factors in many practical situations. In this report, an

analytical investigation of the effects of surface roughness on boundary-layer transition is presented.

The effects of surface roughness on the transition process are basically two-fold:

i) Surface roughness can distort the mean velocity and temperature profiles in a laminar boundary layer from their smooth-wall shapes, thus altering the stability characteristics of the boundary layer, and

ii) Surface roughness can introduce additional disturbances within the boundary layer which may lead to earlier transition.

The exact manner in which surface roughness affects the transition location depends on the type of surface roughness present. In this report, three different types of surface roughness are investigated; distributed roughness, surface waviness, and a single isolated "bump."

In Section 2, the effects of distributed roughness are discussed in some detail starting with a brief reconstruction of the physical model. The perturbation to the mean flow profile is modeled by an enhanced momentum and heat transfer near the surface, which may be considered as resulting from the unsteadiness in the flow over the surface irregularities. This augmented momentum and heat transfer, when interpreted in a statistical sense, gives rise to the concept of a "roughness sublayer" situated between the surface and the outer laminar portion of the boundary layer. This roughness sublayer alters the mean velocity and temperature profiles within the laminar portion of the boundary layer. The distributed roughness model is validated by comparing with Achenbach's experimental results in Subsection 2.2. The model is then applied to a realistic body shape to illustrate its predictive capability in a more quantitative manner. The incorporation of this model into the existing TAPS code in order to provide the technical community with the additional capability of including vehicle surface roughness conditions into performance predictions is described in Section 3.

In addition to distributed roughness, other types of surface roughness which are considered here are two-dimensional waviness and a single, isolated bump. Although waviness and single roughness elements will affect transition through the same two basic mechanisms mentioned above, the details of the mechanisms

which are involved are quite different, and revised roughness models are required in order to include these types of surface irregularities. Again, the perturbed mean flow profiles are expected to lead to earlier boundary-layer transition.

Although the modification of the boundary layer's mean flow profile by roughness elements is expected to be the dominant effect, the increased disturbance level within the boundary layer is also important and should be included. A parametric study of the effect on the boundary layer of varying intensity and spectral content of the disturbances should be performed and the connection between a given surface condition and the magnitude of these parameters needs to be found. These considerations, however, have not been incorporated into the present investigation for lack of a definitive physical correspondence between the surface conditions and the factors influencing the disturbance level within the boundary layer.

2.0 EFFECTS OF DISTRIBUTED ROUGHNESS ON BOUNDARY-LAYER TRANSITION

2.1 A Brief Description of the Roughness Model

A physical model for evaluating the effects of distributed surface roughness on transition characteristics was originally developed and discussed by Kosecoff, Ko and Merkle (1976). In order to facilitate the present discussion, a brief description of the model is given in this section. Detailed derivations and the background of this particular model formulation are given in the original reference.

In this model, the roughness elements are assumed to induce an enhanced momentum and heat transfer near the surface. The enhanced momentum and heat transfer are incorporated into the equations of motion by means of a momentum diffusivity, ε_m, and a thermal diffusivity, ε_H. The momentum diffusivity is assumed to be

$$\varepsilon_m = \varepsilon_{max}\, e^{-\beta_1 (y/k)^2} \tag{1}$$

where β_1 is a constant (which, effectively, determines the "roughness sub-layer thickness), y is the distance away from the wall in the normal direction measured from the bottom of the roughness elements, k is the roughness height, and ε_{max} is the amplitude of the momentum diffusivity at the wall which is represented by the following:

$$\varepsilon_{max} = K_\varepsilon \nu_k Re_k \left[1 - \exp(-Re_k/A^+)\right] . \tag{2}$$

Re_k is the roughness Reynolds number defined by

$$Re_k = u_k k/\nu_k, \tag{3}$$

where the subscript k denotes a quantity evaluated at y = k, K_ε is a constant, and A^+ is a threshold roughness Reynolds number. Obviously, for $Re_k < A^+$, the effects of roughness diminish exponentially.

The thermal diffusivity is defined in terms of a turbulent Prandtl number, Pr_t, so that

$$\varepsilon_H = \varepsilon_m / Pr_t \ . \tag{4}$$

The two quantities ε_H and ε_m are incorporated into the momentum and energy equations by means of an effective viscosity and an effective thermal conductivity which are defined as

$$\mu_t = \mu + \rho\varepsilon_m \tag{5}$$

$$K_t = K + \rho C_p \varepsilon_H \tag{6}$$

where μ and K are the molecular viscosity and thermal conductivity, ρ is the fluid density, and C_p is the specific heat. To incorporate the effects of surface roughness in the boundary-layer calculation, the viscosity, μ, and the conductivity, K, are replaced by their rough-wall counterparts, μ_t, and K_t.

In the numerical evaluation of the effect of distributed roughness, it is assumed that the turbulent Prandtl number is approximately one (i.e., $\varepsilon_H = \varepsilon_m$) and the following values have been determined for the constants appearing in the model:

$$\begin{aligned} K_\varepsilon &= 0.094 \\ A^+ &= 40 \\ \beta_1 &= 1 \end{aligned} \tag{7}$$

2.2 Validation of the Model - Achenbach's Experiment

Very little experimental information on the effect of distributed surface roughness on transition has been reported. It is generally accepted that distributed roughness causes transition to occur earlier than it would on a smooth wall, but it is difficult to find quantitative measures of this shift, even for the most simple flow fields. Because of this lack of data, our distributed roughness model has been compared with only a limited number of experimental results, including the transition data reported by Feindt (1957), and the nosetip

transition results which were obtained in the ABRES reentry program (Merkle, 1976). In the comparisons with Feindt's data, the model provided correct qualitative (as well as reasonably accurate quantitative) predictions of the combined effects of roughness and pressure gradient (both favorable and unfavorable) on the location of transition (Feindt's zero-pressure gradient results were used to complete the calibration of the constants in the model). With regard to the reentry vehicle nosetip data, the model again predicted the correct qualitative, and reasonably accurate quantitative, effects of roughness on the location of transition in the presence of several simultaneous effects such as severe surface cooling, strong pressure gradients, boundary-layer blowing at the surface (simulated ablation), and changes in nosetip geometry. Additional experimental data which have not previously been used for comparative purposes are the results reported by Achenbach (1971). Since these experimental results encompass variations of nearly two orders of magnitude in the unit Reynolds number, they represent a meaningful additional test of the ability of the model to predict the effects of distributed roughness on the location of transition. Accordingly, the model has been applied to the configuration which was tested by Achenbach, and the predictions of the model have been compared with the experimental measurements.

The Achenbach Experiment

Achenbach's experiments include the measurement of the location of transition on a circular cylinder immersed in a crossflow at different freestream Reynolds numbers. The Reynolds number based on the diameter of the cylinder (150 mm) was systematically varied between 6.0×10^4 and 4.0×10^6 so that the location of transition ranged from less than 10 degrees from the forward stagnation line to as much as 100 degrees away (on the leeward side of the cylinder). Three different roughnesses were used in the experiment; the first two were constructed by gluing emery paper to the surface of the cylinder, while the third was constructed by brazing spherical particles to the surface. The roughness heights of these three surfaces were estimated by generating a turbulent boundary layer over the surface, measuring the resulting skin friction, and equating the roughness to an equivalent sand grain roughness by means of Nikuradse's data. The roughness

heights, as determined in this manner, were k = 165, 675, and 1350μ (1μ=0.001 mm) The location of transition was determined by measuring the local surface shear stress by means of a probe imbedded in the cylinder. The shear stress at any angular location could be determined by rotating the cylinder about its axis so as to position the probe at the desired angular location. Since the flow near the stagnation region of the cylinder represents a very strong favorable pressure gradient flow field (starting from a Hartree pressure gradient parameter of β=1.0), these data include the simultaneous effects of roughness and pressure gradient on transition.

Mean Flow Properties of the Cylinder Boundary Layer

All transition distances quoted in Achenbach's paper are normalized by the diameter of the cylinder. The use of a local boundary-layer thickness (such as the displacement or momentum thickness) should give considerably more insight into the experimental data because these boundary-layer thicknesses are the proper local lengths with which the roughness height should be compared. In order to estimate the boundary-layer characteristics for Achenbach's experiment, the standard formula for incompressible, inviscid flow about a cylinder was used to estimate the pressure distribution. The boundary-layer characteristics were then computed from a numerical boundary-layer code which was a modification of the code developed by Price and Harris (1972). Figure 1 through 4 show some of the characteristics of the boundary layer as computed for the smooth-wall case. A schematic of the flow around the cylinder is shown in Figure 1 and, as shown in Figure 2, the Reynolds number based on the local boundary-layer displacement thickness remains quite low (generally below 600) in the region where transition was observed. It is interesting to note that these Reynolds numbers are smaller than those corresponding to transition on a smooth flat plate; thus, the presence of the roughness on the cylinder more than offsets the effects of the strong favorable pressure gradient.

The computed momentum thickness of the smooth-wall boundary layer is shown in Figure 3. Note that the momentum thickness is generally less than 75μ, while the smallest roughness height used by Achenbach was 165μ. Thus, the roughness

tested by Achenbach are considered quite large. The third of the smooth-wall calculations, the boundary-layer shape factor, is shown in Figure 4. Note that the shape factor is almost constant over much of the cylinder for the smooth-wall calculation.

When the presence of the 165μ surface roughness is included in the boundary-layer computation, the shape factor increases considerably and varies with both the freestream Reynolds number and the angular location on the cylinder as is also shown in Figure 4. The roughness Reynolds number, Re_k, is shown in Figure 5. Again, the freestream Reynolds number has a strong effect on the roughness Reynolds number. Finally, the momentum thickness distribution for the rough-wall boundary layer is shown in Figure 6. By comparison with Figure 3, it can be seen that roughness has only a small effect on the momentum thickness development, so that the large increase in the rough-wall shape factor is primarily attributable to the change in the displacement thickness.

Stability Calculations and Transition Predictions for Achenbach's Experiments

The neutral stability curve for the boundary-layer on Achenbach's cylinder with a roughness of 165μ, and at a Reynolds number of $Re_D = 4.0 \times 10^5$ is presented in Figure 7. From this figure it may be shown that the critical Reynolds number occurs very close to the forward stagnation line (at about $\phi = 5^o$). When the total growth rate of each of the various disturbance frequencies are computed and the "e^9" transition criterion is used, the transition location as a function of Reynolds number is obtained for the 165μ case; these results are shown in Figure 8 along with faired curves representing the experimental data for the three roughnesses tested by Achenbach.

The comparison shown in Figure 8 indicates that the present roughness model overpredicts the effects of roughness on transition for this case. Part of this overprediction may be attributed to the skin friction transition criterion which was employed by Achenbach. Skin friction is known to be a relatively late indicator of transition (that is, the increase in skin friction generally is observed toward the latter stages of boundary-layer transition), whereas the "e^9" method

attempts to predict the starting, or early, portion of the transition phenomenon. The ambiguity in the roughness height (owing to the "roundabout" procedure which Achenbach used to quantify the roughness height) also introduces an uncertainty into the prediction. For a qualitative assessment of the trend predicted by the present model, the effects of these uncertainties could be lessened.

Finally, the predicted effect of changes in the roughness height on the location of transition is compared with the experimental measurements in Figure 9. Again, the analysis predicts the correct trend for the effects of roughness on the transition location, but it quantitatively overestimates the effects of the roughness.

In summary, because of the uncertainties associated with the Achenbach experiment, a direct quantitative comparison of the transition location could not be made. The calculations do, however, demonstrate a qualitative agreement with the experimentally observed effect of surface roughness on the transition of a boundary layer about a circular cylinder. In general, the predictions given by the present roughness model appear to be somewhat conservative.

2.3 Application of the Distributed Roughness Model to the Boundary Layer on a Realistic Body

Some computations of the effect of distributed surface roughness for a realistic body shape have been completed and are described below. A particular vehicle designated as Body "H" has been chosen for this investigation. The body contour results in a fairly strong favorable pressure gradient over most of its length; details of the body geometry and the (inviscid) surface velocity are given in Figure 10.

For this body it was assumed that the surface temperature was $11^{o}C$ above the ambient water (i.e., $\Delta T = 11^{o}C$) and that the Reynolds number based on the overall length was 300 million. Different roughness levels were investigated to find a "threshold" level at which the roughness began to have a non-negligible effect on the stability characteristics of the boundary layer. The streamwise variation in the Reynolds number based on displacement thickness is shown in Figure 11 for both the smooth-wall case and for a surface roughness of 25μ. As can be seen, surface roughness causes a very modest increase in δ^* compared to the smooth-wall case.

The momentum thickness development for this body is shown in Figure 12, and the ratio of the roughness height to momentum thickness is shown in Figure 13. As can be seen from this latter figure, the growth of the boundary layer from its relatively thin value at the stagnation point indicates that a threshold roughness level is a function of distance along the body. Small roughness can have substantial effects near the forward portion of the body but they will be effectively buried beneath the boundary layer by the middle of the body. In particular, note that for the 25μ surface roughness case $k/\theta \geq 0.2$ (the value quoted as a roughness threshold in the similar-flow investigations of our previous report) only over the first 15 percent of the body length; the 12.5μ surface roughness results in $k/\theta \geq 0.2$ only over the first 2.5 percent of the body length; and the 2.5μ surface roughness case never results in $k/\theta \geq 0.2$. The corresponding roughness Reynolds numbers are shown in Figure 14. As can be seen from this figure, the roughness Reynolds number increases nearly with the square of the roughness height so that small changes in the roughness height can result in substantial changes in the roughness Reynolds number. Accordingly, small changes in the roughness height can have a sizeable effect on the location of transition. Roughness Reynolds numbers above 30 are noted for the 25μ surface roughness case.

The stability characteristics for the boundary layer about this body for several roughness heights are shown in Figures 15 through 18. Figure 15 shows the neutral stability curve for the smooth-wall case. When a roughness height of 16μ is assumed, the unstable region distorts slightly as shown in Figure 16. A comparison between Figures 15 and 16 indicates that roughness has caused the critical Reynolds number to occur closer to the stagnation point, and has increased the extent of the unstable region, but that the downstream portions of the unstable region are virtually unchanged. This insensitivity to the roughness at the farther downstream stations occurs because the roughness becomes embedded in the boundary layer as it thickens.

When a surface roughness of 25μ is assumed, the critical Reynolds number occurs nearly at the stagnation point and a large, highly-unstable region exists as shown in Figure 17. A comparison between Figures 16 and 17 indicates the strong effect of increasing roughness height on the boundary-layer stability characteristics.

Finally, the integrated disturbance growth rates for these two cases, the 16μ and the 25μ surface roughnesses, are shown in Figure 18. As can be seen, the 16μ surface roughness gives rise to disturbance amplifications as large as e^6. The 25μ surface roughness, however, yields an amplification in excess of e^{13} for all three disturbance frequencies shown. This last figure clearly indicates that the threshold roughness for this body operating at this speed (i.e., the Reynolds number $u_\infty L/\nu = 300 \times 10^6$) and with a wall overheat of 11^oC is about 16μ.

3.0 INCORPORATION OF THE ROUGHNESS MODEL INTO THE TAPS CODE

As described in the previous section, the model for estimating the effects of distributed surface roughness on boundary-layer transition has been developed and validated with experimental data with qualitatively favorable results. The model, however, needs to be validated further with a few well-controlled quantitative measurements before confidence in the model and its associated "constants" can be fully established. At the present time, the model may be used as a qualitative (possibly conservative) guide for estimating the effects of distributed surface roughness for design purpose. Therefore, in order to make the roughness model more readily available to the other investigators in the laminar flow research area, an effort has been devoted in this study to incorporate the roughness model into the TAPS code.

3.1 Analytical Approach

The boundary-layer segment of the TAPS program is based on the Cebeci-Smith (1974) finite-difference boundary-layer program. The general solution procedure used in the program is shown in the diagram below.

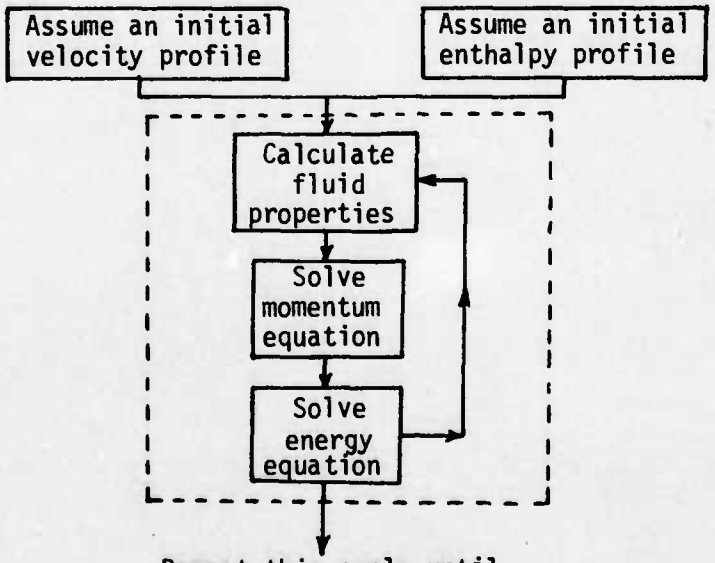

Repeat this cycle until

$$|(f_w'')^{i+1} - (f_w'')^{i}| < \sigma$$

then proceed to the next station.

where f''_w is the velocity gradient at the wall, i is the iteration number and σ is a convergence criterion.

As mentioned in Subsection 2.1, the effects of distributed surface roughness are incorporated by replacing the molecular viscosity and thermal conductivity, μ and K, by their rough-wall counterparts, μ_t and K_t in the momentum and energy equations. Hence, the normalized boundary-layer equations for either two-dimensional or axisymmetric flow can be written as follows (Gentry, 1976):

Continuity

$$\frac{\partial}{\partial x}(r^n \rho u) + \frac{\partial}{\partial y}(r^n \rho v) = 0 \tag{8}$$

Momentum

$$\rho u \frac{\partial u}{\partial x} + \rho v \frac{\partial u}{\partial y} = \rho_e u_e \frac{du_e}{dx} + \frac{1}{r^n}\frac{\partial}{\partial y}\left[r^n\left(\mu_t \frac{\partial u}{\partial y}\right)\right] \tag{9}$$

Energy

$$\rho u \frac{\partial H}{\partial x} + \rho v \frac{\partial H}{\partial y} = \frac{1}{r^n}\frac{\partial}{\partial y}\left\{r^n\left[\frac{K_t}{C_p}\frac{\partial H}{\partial y} + \left(\mu_t - \frac{K_t}{C_p}\right) u \frac{\partial u}{\partial y}\right]\right\} \tag{10}$$

where

- u streamwise (x) component of fluid velocity
- v cross-stream (y) component of fluid velocity
- r radial (or normal) distance from the axis
- ρ density
- n = 0 for two-dimensional flow and
  = 1 for axisymmetric flow
- H total enthalpy
- μ_t total or effective viscosity
- K_t total or effective thermal conductivity
- C_p specific heat at constant pressure
- $( )_e$ conditions at the outer edge of the boundary layer

In order to remove the singularity at x=0, and to stretch the coordinate normal to the flow direction, the Levy-Lees (Hayes and Probstein, 1959) and the Probstein-Elliot

transformations (1956) are used in obtaining the solution of the equations. The transformations are

$$d\xi = \rho_e \mu_e u_e \left| \frac{r_o}{L} \right|^{2n} dx \tag{11}$$

$$d\eta = \frac{\rho u_e}{(2\xi)^{\frac{1}{2}}} \left| \frac{r}{L} \right|^{n} dy \tag{12}$$

$$r = r_o + y \cos \alpha \tag{13}$$

where r_o is the body radius and α is the angle that the surface makes with the body axis.

To simplify the procedure for incorporating the roughness model, the roughness height k is expressed in the transformed coordinate η. Thus, at a given streamwise position, the value of η at the top of the roughness is

$$\eta_k = \frac{u_e}{L(2\xi)^{\frac{1}{2}}} \int_0^k \rho r dy$$

$$\simeq \frac{\rho_e u_e}{L(2\xi)^{\frac{1}{2}}} \left[k\, r_o + \frac{k^2}{2} \cos \alpha \right] \simeq \frac{\rho_e u_e}{L(2\xi)^{\frac{1}{2}}} \left[k\, r_o \right] \quad . \tag{14}$$

Once the roughness height is defined in the transformed coordinate system, its effect can be computed at each streamwise location. The procedure used for incorporating the roughness model into the TAPS program is described below in conjunction with Figure 19.

1. The computation will include the effect of surface roughness if the control flag LG23 = 3 in the input data.
2. Input data should include the roughness height k along the body surface.
3. Calculate the roughness height k in the transformed coordinate η.

4. Obtain the variations of velocity u, temperature T, viscosity μ, density ρ in the cross-stream (η) direction from the TAPS boundary-layer flow calculation.

5. Calculate the roughness Reynolds number Re_k.

6. Calculate the momentum diffusivity ε_m and thermal diffusivity ε_H according to the roughness model.

7. Obtain the total or effective viscosity μ_T and thermal conductivity K_T.

8. Replace the molecular viscosity, μ, and conductivity, K, by their rough-wall counterparts μ_T and K_T in the momentum and energy equations.

9. Resume the boundary-layer calculation in the TAPS computer program.

3.2 Descriptions of the Changes in the TAPS Code

Modification of the Input Data

The Input Data format is the same as the original TAPS Input format except for the following changes:

i) Flag Control Card

Column	Code	Routine	Format	Explanation
23	LG23	INP2	I1	Laminar flow roughness control flag = 0 smooth surface = 3 roughness height k is input on the boundary-layer station data card

ii) Boundary-Layer Station Data Cards

Column	Code	Routine	Format	Explanation
41-46	RP(I)	INP2	F6.0	Equivalent sand-grain roughness height for laminar flow, inches

(NOTE: The original TAPS Code has the same input format for turbulent flow calculations.)

A sample of the input data is shown in Table 1.

Modification of the TAPS Program

The structure of the TAPS Boundary-Layer Program is presented in Table 2. The primary modifications to the computer program are in the FLP2 Subroutine for the calculation of the fluid properties. These modifications are shown in Tables 3-1 and 3-2. Subroutine OTPT also has been modified as shown in Table 3-3 in order to simplify the output format. A sample of the output summary is presented in Table 4.

3.3 Discussion of the Results

Calculations on the effects of distributed roughness for the Body "H" have been performed by using the modified TAPS code. A comparison of the results with those calculation in Section 2 is presented in Figure 20 through Figure 22.

In general, results from the two codes are in fairly good agreement. For the smooth-wall case, the variation in the two computed momentum thicknesses is only 2% at x/L = 0.4. The effects of surface roughness on the roughness Reynolds number Re_k and the parameter k/θ are presented in Figures 21 and 22. For the small roughness height k = 12.5μ, the discrepancies from the two codes are negligible. For the roughness height k = 25μ, the resulting Re_k and k/θ from Harris' code are slightly higher than the results from TAPS. In Subsection 2.2, it was concluded that the analysis from Harris' code quantitatively overpredicted the effects of roughness at k = 165μ (the experimental data of Achenbach). Therefore, by intuition it is anticipated that the roughness model in the TAPS code should yield a better agreement with experimental data than Harris' code.

4.0 SOME PRELIMINARY CONSIDERATIONS ON OTHER TYPES OF SURFACE ROUGHNESS

Thus far, the analytical effort at assessing the effects of surface roughness on the location of boundary-layer transition has dealt with distributed roughness only. The basic mechanism envisioned in that model is an enhanced momentum and heat transfer near the wall as a result of the unsteady flow downstream of each distributed roughness element. This effect of surface roughness is manifested through the change of the stability characteristics of the modified mean flow profiles within the laminar portion of the boundary layer. An implicit requirement of this model is the presence of a separated flow region behind each roughness element. A lower bound cut-off of $Re_k = u_k k/\nu_k = 40$ has been used in the model to account for the non-existence of a separated region, and, therefore, the absence of unsteady flow at roughness Reynolds numbers below this value. This characteristic value was assumed to be the same as the incipient Reynolds number for the unsteady wake flow behind a cylinder. The arbitrariness of this cut-off and the need for examining the effects of surface roughness without flow separation in order to assess the minimum critical roughness height with more confidence have led us to examine and to formulate the problem for the effect of a wavy wall as summarized below. The intent is to provide a lower bound on the effect of roughness as well as to simulate the frequently postulated machining-induced, organized surface roughness.

For larger roughness heights under practical conditions, a model of isolated two-dimensional and/or three-dimensional roughness elements is more representative. Their effect on boundary-layer transition is often observed to be significant and to dominate. In Subsection 4.2, we present a brief review and attempt to investigate the effect of an isolated two-dimensional roughness element using the triple-deck formulation of Smith (1973).

4.1 Wavy Wall

The Effect of a Wavy Wall on the Mean Flow Profiles

Recently, Lessen and Gangwani (1976) have presented an analysis of the flow over a wavy wall. Their analysis restricts the wavelength of the roughness to be small compared with the wavelength of a Tollmien-Schlichting wave, and, in addition, restricts the height of the roughness so that the wall angles are shallow and separation does not occur behind the individual bump. Viscous flow over a wavy wall causes a mean distortion to the flow field (if second order terms are kept) which will, in turn, affect the stability characteristics of the boundary layer. Since this mechanism for distorting the mean flow is a steady-flow mechanism, its effect is not included in the distributed roughness model which applied to roughness elements whose height is comparable to their characteristic wavelength. The unsteady flow effects of the distributed roughness model are expected to dominate the second-order steady flow distortions which are predicted by Lessen's analysis when the roughness is large, but, in the limit when the roughness heights are small, the latter effect may be the more important. The purpose of reviewing Lessen's analysis is to determine whether his analysis predicts a more significant effect of roughness in the very small roughness-height region where laminar flow underwater bodies are expected to operate.

In the wavy-wall analysis, the flow field is divided into three separate parts, a distorted, spatially averaged mean flow, a steady perturbation at a wavelength corresponding to that of the wavy wall, and an unsteady Tollmien-Schlichting wave. In order to keep the analysis simple, and to cast emphasis upon the effects of the wall waviness on the stability characteristics of the flow, the T-S waves will be treated as being infinitesimal in strength (i.e., they are considered as being linear in a traditional "e^9" sense), while the roughness amplitude is taken as being small, but finite. In the analysis, the distorted mean flow will be denoted by a variable with an over-bar, the periodic perturbation due to the roughness will be denoted by a superscript asterisk, and the T-S wave will be indicated by a prime. Other symbols are taken as standard: u and v are the velocity components in an x-y cartesian coordinate system, the pressure divided

by the density is indicated by p, and the kinematic viscosity by ν. Thus, the streamwise velocity component is written as

$$u = \bar{u} + u^* + u' \ . \tag{15}$$

If expressions of the form of Equation (15) are introduced into the Navier-Stokes equations, and the flow field is averaged over time and over one wavelength of the roughness, the equations for the mean flow become

$$\bar{u} \frac{\partial \bar{u}}{\partial x} + \bar{v} \frac{\partial \bar{u}}{\partial y} + \frac{\partial \bar{p}}{\partial x} = \nu \frac{\partial^2 \bar{u}}{\partial y^2} - \frac{\partial}{\partial y} \langle u^* v^* \rangle \tag{16}$$

$$\frac{\partial \bar{u}}{\partial x} + \frac{\partial \bar{v}}{\partial y} = 0 \ , \tag{17}$$

where the boundary-layer approximations have been applied, and the second order quantities in the roughness-induced distortion (but not the T-S wave as indicated above) have been retained. The symbol, $\langle\ \rangle$, is used to indicate the spatial average over one wavelength of the roughness. By again returning to the complete Navier-Stokes equations, introducing Equation (15), time averaging, subtracting Equations (16) and (17), and applying parallel-flow approximations, we obtain the equations governing the perturbation induced by the roughness:

$$\bar{u} \frac{\partial u^*}{\partial x} + \frac{\partial \bar{u}}{\partial y} v^* + \frac{\partial p^*}{\partial x} = \nu \nabla^2 u^* \tag{18}$$

$$\bar{u} \frac{\partial v^*}{\partial x} + \frac{\partial p^*}{\partial y} = \nu \nabla^2 v^* \tag{19}$$

$$\frac{\partial u^*}{\partial x} + \frac{\partial v^*}{\partial y} = 0 \ . \tag{20}$$

This system of equation is identical to that which governs Tollmien-Schlichting waves, except that the unsteady terms are not present. As will be seen later, the boundary conditions corresponding to this equation system are non-homogeneous so that non-trivial solutions to Equations (18) and (20) can be found. Note that a linear approximation to this set of equations is sufficient in order to maintain the Reynolds stress term which appears in the mean flow equation (16); the Reynolds stress term $\langle u^* v^* \rangle$, is non-zero because of the presence of the mean shear $\bar{u}\,(y)$.

The equations for the Tollmien-Schlichting wave are obtained by standard techniques and have the standard form except that the mean flow coefficients which appear in the Orr-Sommerfeld equation are those of the distorted mean flow as computed from Equations (16) and (17).

The analysis of the flow over a wavy wall is completed by specifying the boundary conditions for the three systems of equations. These boundary conditions, which can be obtained by expanding the solution in a Taylor's series at the wall, are as follows: the boundary condition for the mean flow is

$$\bar{u}(0) = -\frac{1}{2}\langle y_w^2\rangle\, \bar{u}_{yy}(0) - \langle y_w u_y^*(0)\rangle \tag{21}$$

where y_w is the amplitude of the roughness; the boundary conditions for the roughness induced disturbance is

$$u^*(0) = y_w \bar{u}_y(0)\ ; \tag{22}$$

while the boundary conditions for the Tollmien-Schlichting wave are the standard homogeneous ones, both at infinity and at the wavy wall surface.

Some effects of the wavy wall on the critical Reynolds number are given in Figure 23. These results have been computed by Lessen; results for higher Reynolds numbers are not available. As can be seen, roughness is destabilizing, and, if the limits of the analysis are severely strained, changes of about 10 percent can be noted in the critical Reynolds number.

Lessen's model has been extended to include the effects of pressure gradient and surface heat transfer. Some preliminary order of magnitude estimates have been made for the effect of surface heating combined with a wavy wall. These results, which are for wavelength-to-height ratios which ensure that the flow remains attached, have indicated that heating has a very weak effect on stability and transition in this circumstance. Consequently, our net assessment for the effect of surface roughness on stability is that even in the limit of very small "roughness" heights, waviness never dominates the distributed roughness effect

(for similar values of roughness height). Therefore, we may consider the threshold roughness height established with the distributed roughness model to be conservative. Further investigation of the effect of a wavy wall appears unwarranted at the present time.

4.2 Single Two-Dimensional Bump

The effects of a single two-dimensional bump on the boundary-layer mean-flow profile have been considered by Smith (1973) who used a "triple-deck" analysis to determine its effects. The triple deck-analysis expands the equations in terms of a small parameter ε, which is defined as

$$\varepsilon = Re_{\delta}^{-\frac{1}{4}} \tag{23}$$

where δ is the local boundary-layer thickness. The height of the bump is of order $\varepsilon\delta$ and its width must be of order δ/ε. Asymptotic equations are written for each of these regions and proper matching procedures are used to determine the interaction between the three regions.

In Smith's analysis, the inner region extends from the wall to a height which is similar in order of magnitude to that of the bump, $O(\varepsilon\delta)$. The main or middle deck constitutes the remainder of the boundary layer and has a thickness of the order of δ. The upper deck extends to a height of the order of δ/ε, and, being outside the boundary layer, accounts for the interaction between the inviscid flow and the bump.

The detailed results of the triple-deck analysis show that the predominant effect of the bump on the boundary layer is to cause a local distortion in the impressed pressure gradient. The effects of the bump are, however, largely local and decay to small levels within a length on the order of a bump width. The net distortion in the profile which exists downstream of the bump is, therefore, quite small. The analysis does, however, show that the boundary-layer formulation is adequate for flows over bumps of this nature, but that the interaction with the inviscid flow must be included in the analysis. The details of including the viscous/inviscid interaction require a level of difficulty which is

almost identical to computing the complete boundary-layer equations numerically. Consequently, the effects of the bump can equally well be included by using a standard numerical boundary-layer scheme and using proper step size resolution in the vicinity of the bump. In so doing, the perturbation to the local pressure gradient must, of course, be included in the computation.

In the recent Westinghouse tow-tank tests the effect of a single two-dimensional bump such as that described above was examined. The following is an analysis of its effect on the boundary layer and its transitional characteristics.

Effects of a Single Two-Dimensional Bump on Transition

The effects of a single bump on the location of transition may be handled quite differently from an analytical viewpoint than the case of multiple bumps (distributed roughness or wall waviness). For the single bump case, it is possible to resolve the details of the distortions near the location of the bump and include them in both the boundary layer and stability calculations. Consequently, as an augmentation of our wavy-wall and distributed roughness analyses, we are also reviewing the effects of a single two-dimensional bump on the location of transition.

For this analysis, rather than consider a general case, we have restricted our attention to a specific bump of given geometry on a particular body. The specific bump which we are considering is the one which was installed upon the Reichardt body in the recent MBT[3] tow tank tests (Westinghouse, 1977). Our intent is to compare the analytical predictions of its effect on transition with the observed experimental results. The geometry of this particular bump and its location on the vehicle are shown in Figure 24. As can be seen from the figure, the height of the bump is 0.125 mm and its length is about 38 mm. At the critical velocity of 5.69 m/sec the undisturbed boundary-layer momentum thickness at this location is computed to be about 0.15 mm. Thus, the bump height is slightly smaller than the local momentum thickness of the boundary layer, and is about 250 boundary-layer (momentum) thicknesses long.

A single bump of this character can affect the location of transition through at least three distinct mechanisms. First of all, the bump introduces a local perturbation to the boundary-layer velocity field which alters the stability characteristics of the boundary layer. This aspect of a bump was reviewed in terms of a triple-deck analysis (Smith, 1973) which indicated that the use of boundary-layer theory in the vicinity of the bump was acceptable so long as the local pressure perturbation is taken into account. The second effect is that the bump, which was composed of silver epoxy, may not have reached the same surface temperature overheat as the rest of the wall even though it is a reasonably good heat conductor. Finally, the local geometrical characteristics of the surface which are introduced by the bump have regions of concave curvature near the front and the back sides of the bump, and these regions could stimulate the growth of Taylor-Görtler vortices which, in turn, could lead to transition at substantially lower amplification ratios than the "e^9" criterion.

The profile of the surface wave which is shown in Figure 24 can, to a first approximation, be represented as

$$y = \frac{h}{2}\left(1 - \cos\frac{2\pi}{\lambda} S\right) \tag{24}$$

where the bump height, h, is 0.125 mm and the bump length, λ, is 38.0 mm. Considering first the Taylor-Görtler instability, we compute a maximum concave curvature of $\zeta = 1.72 \times 10^3$ mm^{-1} at S = 0 and λ. For a vehicle velocity of 5.69 m/sec (11 knots), the Görtler parameter, G_c (= $Re_\theta\sqrt{\theta\zeta}$), at this location is $G_c = 12.7$. Stability calculations indicate Taylor-Görtler instabilities become manifest when the parameter G_c exceeds a value of 1 or 2, and this would suggest that Görtler instabilities could be present near the bump. We note, however, that the sinusoidal representation of the shape of the bump is only an approximation and that the actual shape (and, hence, the curvature) remains undetermined. Nevertheless, the above calculation should have the correct order of magnitude, and a strong likelihood of instability is indicated. The reason for the possible appearance of a Taylor-Görtler instability is, of course, directly related to the high value of Re_θ for the boundary layer which was computed for the body flow; this sensitivity is common in all high Reynolds number tests.

The pressure coefficient in the neighborhood of the bump is shown in Figure 25. In the absence of the bump, the pressure coefficient is virtually constant, but with the bump present, a characteristic adverse pressure gradient, followed by a favorable and then a second adverse pressure gradient region results. When translated into boundary-layer characteristics, the boundary layer is actually thinned somewhat in the favorable pressure gradient region, as shown on Figure 26, but the net effect of the bump is to leave the boundary layer somewhat thicker downstream of the bump as compared to the undistorted case.

Some preliminary stability calculations in which the pressure perturbation has been included, and for which it is assumed that no surface heat transfer takes place in the vicinity of the bump, have been obtained. These results indicate that the effect of the two perturbations taken together (no surface heating plus pressure gradient effects) are sufficient to cause a noticeable change in the stability characteristics and to force transition to occur at the bump. These preliminary analyses should be further expanded in the future in order to obtain a more definitive assessment of the effects of an isolated bump on boundary-layer transition.

5.0 SUMMARY

In this report, we have presented a summary of our recent investigations of the effects of surface roughness on boundary-layer transition. The primary effort has focused on the formulation, validation and application of the enhanced momentum and heat transfer model for distributed roughness elements. Without further quantitative experimental confirmation of this model, it is our present opinion that this model, which has been incorporated into the TAPS code, can provide a reasonable prediction of the effects of randomly distributed surface roughness on the transition location for a realistic underwater vehicle. The model, in particular, points out the reduced effectiveness of surface heating for delaying boundary-layer transition in the presence of surface roughness. The second type of surface irregularity considered was waviness which could result during vehicle construction. The model of Lessen and Gangwani has been extended to provide a qualitative assessment of this effect. The preliminary results, however, suggest a weak influence for expected surface waviness parameters such as when the wave height to wave length ratio is small. Additional effort is needed to examine the effect of surface waviness in a more quantitative manner and should include relatively high wave height to wave length ratios for which the flow may no longer remain attached everywhere on the surface.

The third type of surface irregularity considered was a single, two-dimensional bump. The triple-deck formulation of Smith was used to investigate the effect on the mean flow profiles within the boundary layer and, therefore, the stability characteristics. This analysis is quite preliminary in nature and additional effort is needed before any quantitative assessment can be made.

In summary, we believe that surface irregularities can play a dominant role in determining the practical range of applicability of advanced laminar-flow techniques. Extreme care should be taken in the interpretation of experimental results if quantitative information on the surface finish conditions is not known. The present phenomenological model for distributed surface roughness, however, can be used for a first-order estimate of the transition location.

Based on the qualitative comparison with the existing experimental results, we would deduce that the present model would provide a rather conservative estimate of the effects of surface roughness. A more quantitative assessment, however, must rely on additional validations with carefully performed surface roughness experiments. These experiments are critically needed for an improved understanding of the effects of surface roughness on the boundary-layer transition.

ACKNOWLEDGEMENTS

The authors would like to express their deepest appreciation to Dr. D. R. S. Ko for his skillful guidance and helpful advice during the course of this study. Sincerest appreciation is also extended to Dr. R. L. Gran, Mr. W. W. Haigh and Mr. A. M. O. Smith for their invaluable suggestion and assistance in the preparation of this final report. Dr. C. L. Merkle, the initial project engineer for this program, left DynaTech prior to the completion of this study.

REFERENCES

Achenbach, E. (1971), "Influence of Surface Roughness on the Cross-Flow around a Circular Cylinder," J. Fl. Mech., Vol. 46, Part 2, pp. 321-335.

Cebeci, T. and Smith, A. M. O. (1974), Analysis of Turbulent Boundary Layers, Academic Press, New York.

Feindt, E. G. (1957), "Untersuchungen über die Abhängigkeit des Umschlages Laminar-Turbulent von der Oberflachenrauhigkeit und der Druckverteilung," Gesellschaft, Vol. 50, pp. 180-203.

Gentry, A. E. (1976), The Transition Analysis Program System, Volume 1 — User's Manual, McDonnell Douglas Report No. MDC J7255/01.

Gentry, A. E. and Wazzan, A. R. (1976), The Transition Analysis Program System, Volume II — Program Formulation and Listings, McDonnell Douglas Report No. MDC J7255/02.

Hayes, W. D. and Probstein, R. F. (1959), Hypersonic Flow Theory, Academic Press, New York and London, 290 p.

Kosecoff, M. A., Ko, Denny, R. S. and Merkle, C. L. (1976), An Analytical Study of the Effect of Surface Roughness on the Stability of a Heated Water Boundary Layer, Physical Dynamics, Inc., PDT-76-131.

Lessen, M. and Gangwani, S. T. (1976), "Effect of Small Amplitude Wall Waviness upon the Stability of the Laminar Boundary Layer," The Physics of Fluids, Vol. 19, No. 4.

Merkle, C. L. (1976), Stability and Transition in Boundary Layers on Reentry Vehicle Nosetips, Flow Research Report No. 71, Kent, WA.

Price, J. M. and Harris, J. E. (1972), Computer Program for Solving Compressible Nonsimilar Boundary-Layer Equations for Laminar, Transitional, or Turbulent Flows of a Perfect Gas, NASA Langley Research Center Technical Memorandum X-2458.

Probstein, R. F. and Elliott, D. (1956), "The Transverse Curvature Effect in Compressible Axially Symmetric Laminar Boundary-Layer Flow," J. Aeron. Society.

Smith, F. T. (1973), "Laminar Flow over a Small Hump on a Flat Plate," J. Fl. Mech., Vol. 57, Part 4, pp. 803-824.

Westinghouse Electric Corporation (1977), Multiple Body Two Tank Test Results, Westinghouse Ocean Engineering Report No. 77-13 (Confidential).

Table 1. Sample Input Data for Roughness Model in TAPS Code.

```
0         1         2         3         4         5         6         7         8
12345678901234567890123456789012345678901234567890123456789012345678901234567890
00
4
  10                                                    0
01100 1        0001 00 00030000 3                     78 85      0  BODY-H, K=.00050(IN)
.005       .030       1.0
+507.69000E+00                    +5.8196000E+06
+1.0000000E+00+1.0000000E+00+84.500000E+00+0.5000000E+00+5.5005000E+00
 0.00000 0.000001.0000      527.69          .00000
  .01199   .01200 .8480      527.69          .00000   <-- Input k = 0 for the first
  .03597   .03600 .7335      527.69          .00050       two stations.
  .06651   .06662 .5174      527.69          .00050
  .11256   .09700 .3400      527.69          .00050
  .16844   .12236 .2741      527.69          .00050
  .22347   .14317 .2464      527.69          .00050
  .29902   .16864 .2269      527.69          .00050
  .41608   .20420 .2132      527.69          .00050
  .55360   .24224 .1996      527.69          .00050
  .69101   .27758 .1950      527.69          .00050
  .82874   .31164 .1886      527.69          .00050
  .96643   .34461 .1828      527.69          .00050
 1.13837   .38451 .1786      527.69          .00050
 1.37890   .43899 .1727      527.69          .00050
 1.65381   .49968 .1670      527.69          .00050
 1.92896   .55928 .1635      527.69          .00050
 2.20392   .61841 .1575      527.69          .00050
 2.47882   .67661 .1538      527.69          .00050
```

Table 2. Structure of the TAPS Boundary-Layer Program

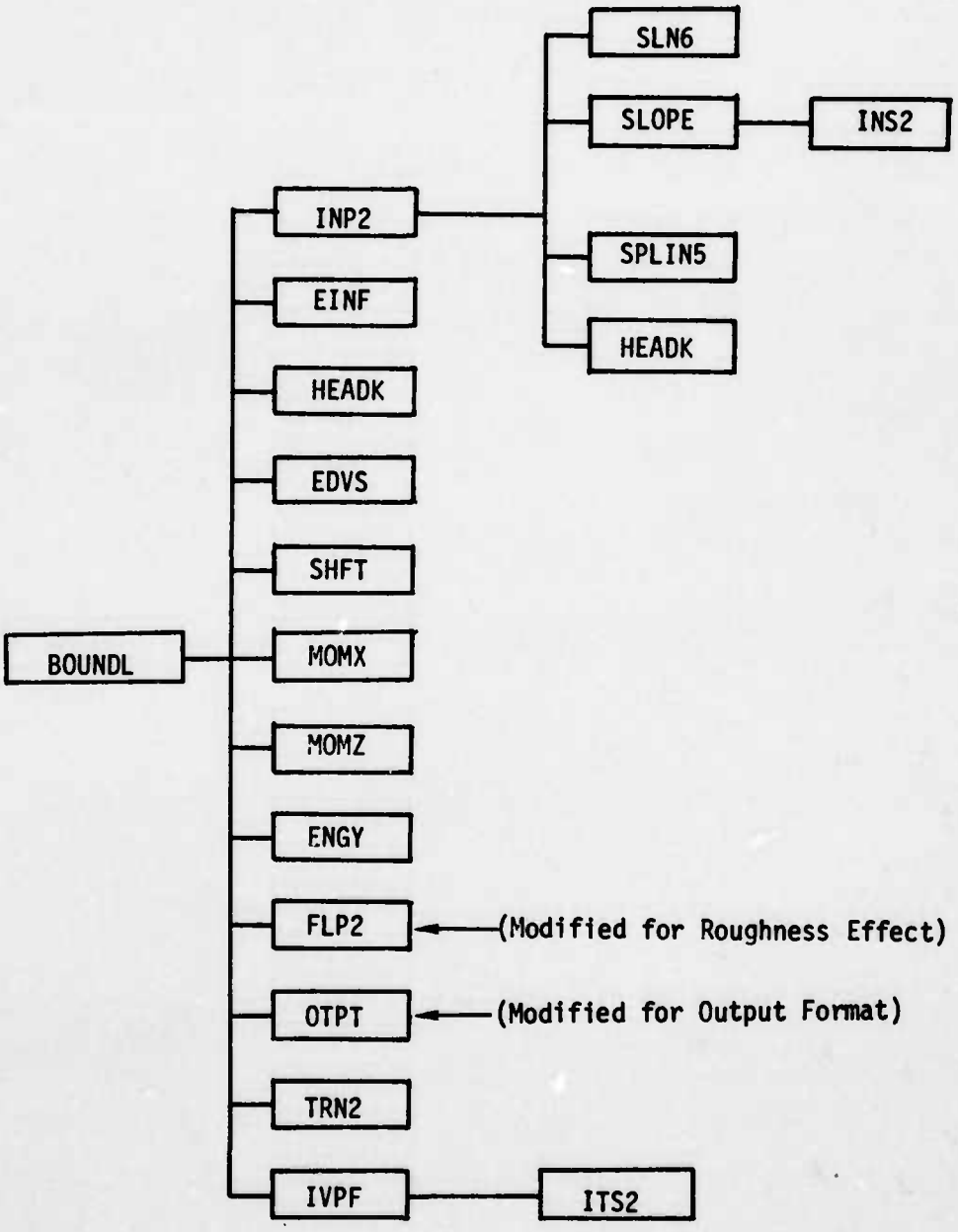

Table 3-1. FORTRAN Program Change in SUBROUTINE FLP2.

```
     2           ,BR(150),TE(150),RHOE(150),RMUE(150),GW(150),GPW(150)   FLP2
     3           ,RF1(150),YS(150),IGX1(150),FPW(150),ROL(150),PRES      FLP2
      COMMON/BL19/C(200,2),G(200,2),GP(200,2),                           FLP2
     1           RHO(200),RMU(200),TVCT(200),RKA(100),AK(200),ACP(200)
      DATA    SHLO/3.E03/  , SHHI/36.E06/                                FLP2
      A1 = 0.                                                            FLP2
      IF(XI(NX) .GT. 0.) A1 = SQRT(2.*XI(NX))/(RHOE(NX)*UE(NX))          FLP2
      VESQ = UE(NX)**2 + WE**2                                           FLP2
         .


  100 CONTINUE                                                           FLP2
      TEMP   = G(I,2) * TI                                               FLP2
      TTREF  = TEMP / 491.69                                             FLP2
      TTREF2 = TTREF * TTREF                                             FLP2
      TTREF3 = TTREF2* TTREF                                             FLP2
      TTREF4 = TTREF3* TTREF                                             FLP2
      IF (LG03 .EQ. 2) GO TO 110                                         FLP2
      AK(I)=6.917333E-02*(-1.9410583+5.2220185*TTREF
     1 -2.693322*TTREF2+0.4176176*TTREF3)
      ACP(I)=25222.98*(1.4833689
     1 -0.8072501*TTREF+0.3289607*TTREF2)
      RHO(I) = 1.9400 * (.8039244.4615901*TTREF-.2869774*TTREF2          FLP2
     1         +.0234689*TTREF3)                                         FLP2
      IF (LG04 .EQ. 1) RHO(I) = RHOE(NX)                                 FLP2
      RMU(I) = 3.74614E-05 / (35.155539-106.9718715*TTREF+107.7720376    FLP2
     1         *TTREF2-40.5953074*TTREF3+5.6391948*TTREF4)               FLP2
      PRW(I) = 13.66 / (73.376906-208.747538*TTREF+197.7604726*TTREF2    FLP2
     1         -68.9626188*TTREF3+7.4779458*TTREF4)                      FLP2
```

Table 3-2. FORTRAN Program Change in SUBROUTINE FLP2.

```
C---- COMPUTE  RHO, MU, C  FOR INCOMPRESSIBLE FLOWS                    FLP2
  130 RHO(I) = RHOE(NX)                                                FLP2
      RMU(I) = RMUE(NX)                                                FLP2
      C(I,2) = 1.0                                                     FLP2
140   CONTINUE
      IF(LG23.NE.3)GO TO 333
      IF(RP(NX).EQ.0.0)GO TO 333
      ETAKK=RHOE(NX)*UE(NX)*RP(NX)*ROL(NX)/(RL*SQRT(2.*XI(NX)))
      ETAKK=ETAKK/12.0
      DO 220 I=1,NP
      IF(ETA(I)-ETAKK)220,220,222
222   IK=I
      GO TO 230
220   CONTINUE
230   IK1=IK+1
      UKK=U(IK,2)+(U(IK1,2)-U(IK,2))*(ETAKK-ETA(IK))/(ETA(IK1)-ETA(IK))
      RKK=RHO(IK)*UE(NX)*UKK*(RP(NX)/12.0)/RMU(IK)
      RKA(NX)=RKK
      DO 240 I=1,NP
      ESMM=0.094*(RMU(IK)/RHO(IK))*RKK*(1.0-EXP(-RKK/40.0))
      EAAA=(ETA(I)/ETAKK)**2
      IF(EAAA.GE.20.0)GO TO 553
      ESMM=ESMM*EXP(-EAAA)
      GO TO 249
553   ESMM=0.0
249       RMU(I)=RMU(I)+RHO(I)*ESMM
      AK(I)=AK(I)+RHO(I)*ACP(I)*ESMM
      PRW(I)=RMU(I)*ACP(I)/AK(I)
      C(I,2)=RHO(I)*RMU(I)/(RHOE(NX)*RMUE(NX))
240   CONTINUE
333   CONTINUE
      IF(LG18 .EQ. 2)  RF1(NX) = COS(.0174533*RF1(NX))                 FLP2
      SUM = 0.                                                         FLP2
      F1 =  RF1(NX)*RHO(NP)/RHO(1)                                     FLP2
```

Table 3-3. FORTRAN Program Change in SUBROUTINE OTPT.

```
      COMMON /BL17/ RX(150),CFA(150),CF(150),ETAE(150),CDI(150),ST(150),OTPT
     1        INP(150)                                                   OTPT
      COMMON/BL19/C(200,2),G(200,2),GP(200,2),                          OTPT
     1            RHO(200),RMU(200),TVCT(200),RKA(100)
      COMMON /RADIUS/ROMAX,CDRAG(150)                                   OTPT
      DIMENSION  Y(200),  THEDA(150)                                    OTPT

  250 RTHETA=0.                                                         OTPT
      H=0.                                                              OTPT
      CDRAG(1) = 0.0                                                    OTPT
      TWW=(GW(1)-1.0)*TI
      RDELS=0.0
      IF(XI(I) .EQ. 0.)  GO TO 260                                      OTPT
      RTHETA = RX(I)*THETA(I)/XS(I)                                     OTPT
      RDELS=RX(I)*DELS(I)/XS(I)
      TWW=(GW(I)-1.0)*TI
      H      = DELS(I)/THETA(I)                                         OTPT
      IF(RF(I).EQ.0.0) THEPK=0.0
      IF(RF(I).GT.0.0) THEPK=RF(I)/(THETA(I)*12.00)
  260 WRITE(6,510)I,YS(I),XS(I),DELS(I),THETA(I),H,CF(I),THEPK
      IF(FK.GE.1)WRITE(6,520)RX(I),RDELS,RTHETA,TWW,RKA(I),CDRAG(I)
      IF (FK .LT. 1) WRITE (6, 520 ) YS(I),RX(I),RTHETA,H,CFA(I),GPW(I),OTPT
     1                               ST(I),ETAE(I)                    OTPT


  470 FORMAT (1H ,F11.5,6E17.6)                                         OTPT
  480 FORMAT (1H ,30X,16HOUTPUT SUMMARY  ,10A4,/)
  490 FORMAT(///49H   STA     X(FT)      S(FT)       DELS        THETA
     1,28H    H         CF          K/D    /16X
     2,33H     RS           RDELS       RTHETA
     3,28H    DT(F)     RK          CD     )
  500 FORMAT (1H0,/,7X,1HN,12X,4H  S ,13X,5HTHETA,12X,4HDELS,14X,       OTPT
     1        2HCF,14X,4HFPPW,14X,2HGW,15X,4HIMAX,/,1H ,5X,4HX*RL,11X,  OTPT
     2        2HRX,13X,6HRTHETA,14X,1HH,15X,3HCFA,14X,3HGPW,13X,        OTPT
     3        4H ST ,13X,6HETAINF,/)                                    OTPT
  510 FORMAT(/2X,I4,F10.4,3F11.6,F8.4,2F10.6)
  520 FORMAT(16X,3E11.4,F8.2,F10.2,F10.6)
  530 FORMAT (1H ,I3,2X,F10.6,7E16.6)                                   OTPT
      END                                                               OTPT
```

Table 4. Sample Output Summary for Roughness Model in TAPS Code.

OUTPUT SUMMARY

STA	X(FT)	S(FT) RS	DELS RDELS	THETA RTHETA	H DT(F)	CF RK	K/O CD
1	0.0000	0.000000 0.	0.000000 0.	0.000000 0.	0.0000 20.00	0.000000 0.00	0.000000 0.000000
2	.0120	.016963 .3833E+05	.000102 .2314E+03	.000020 .4604E+02	5.0259 20.00	.009295 0.00	0.000000 .000000
3	.0360	.050890 .1523E+06	.000114 .3418E+03	.000042 .1257E+03	2.7193 20.00	.009449 29.90	.991941 .000000
4	.0665	.094195 .3793E+06	.000133 .5340E+03	.000048 .1924E+03	2.7747 20.00	.006060 32.09	.871806 .000000
5	.1126	.149414 .7036E+06	.000155 .7316E+03	.000057 .2704E+03	2.7055 20.00	.003953 31.70	.725613 .000000
6	.1684	.210791 .1041E+07	.000197 .9724E+03	.000073 .3614E+03	2.6909 20.00	.002019 25.74	.569401 .000001

$RS = \frac{u_e S}{\nu}$ DELS = δ^* THETA = θ H = δ^*/θ CF = C_f K/O = k/θ

$RDELS = \frac{u_e \delta^*}{\nu}$ $RTHETA = \frac{u_e \theta}{\nu}$ $DT = T_w - T_\infty$ $RK = \frac{u_k k}{\nu_k}$ CD = C_D

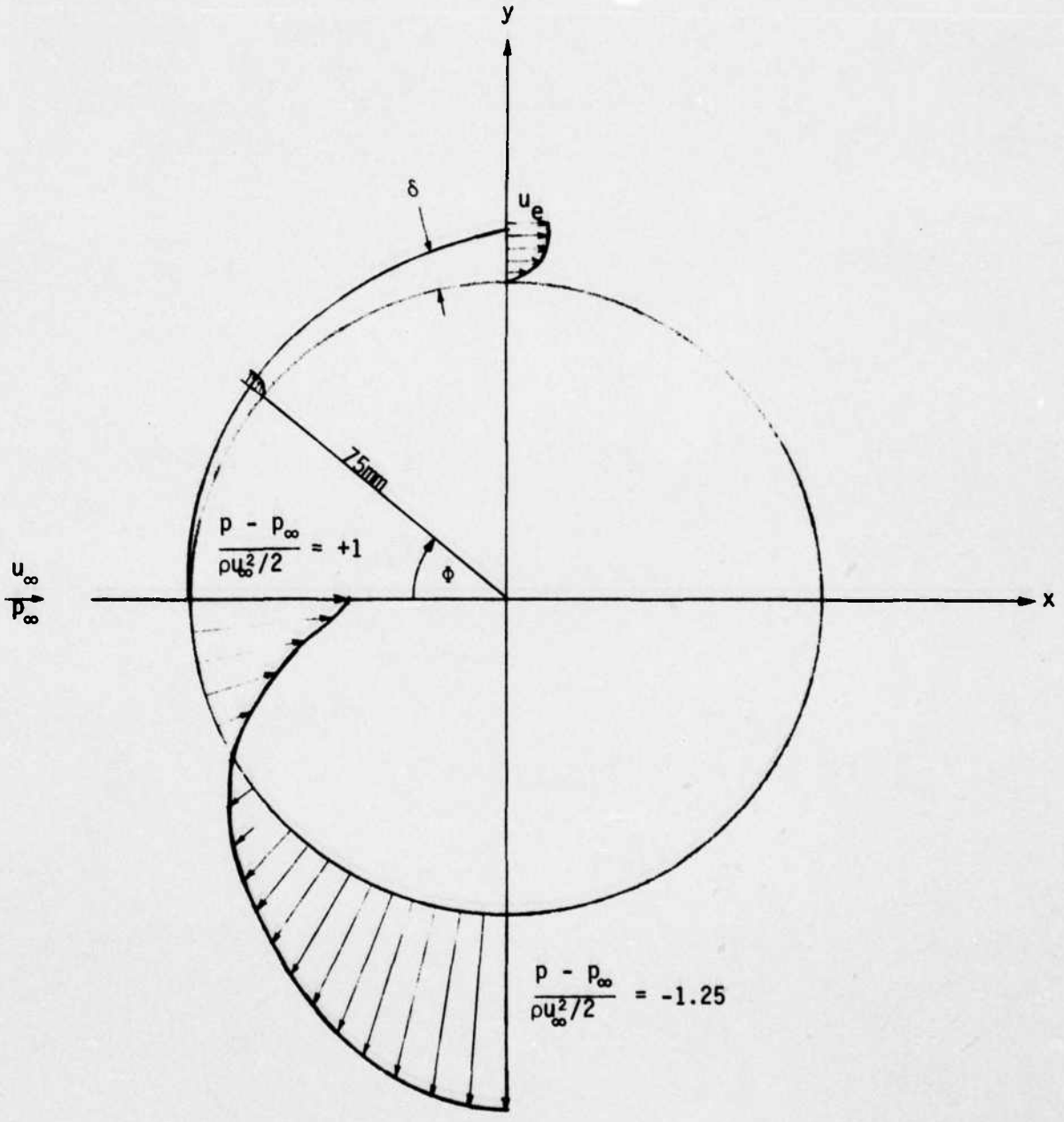

Figure 1. A Schematic Diagram for Flow Past a Cylinder

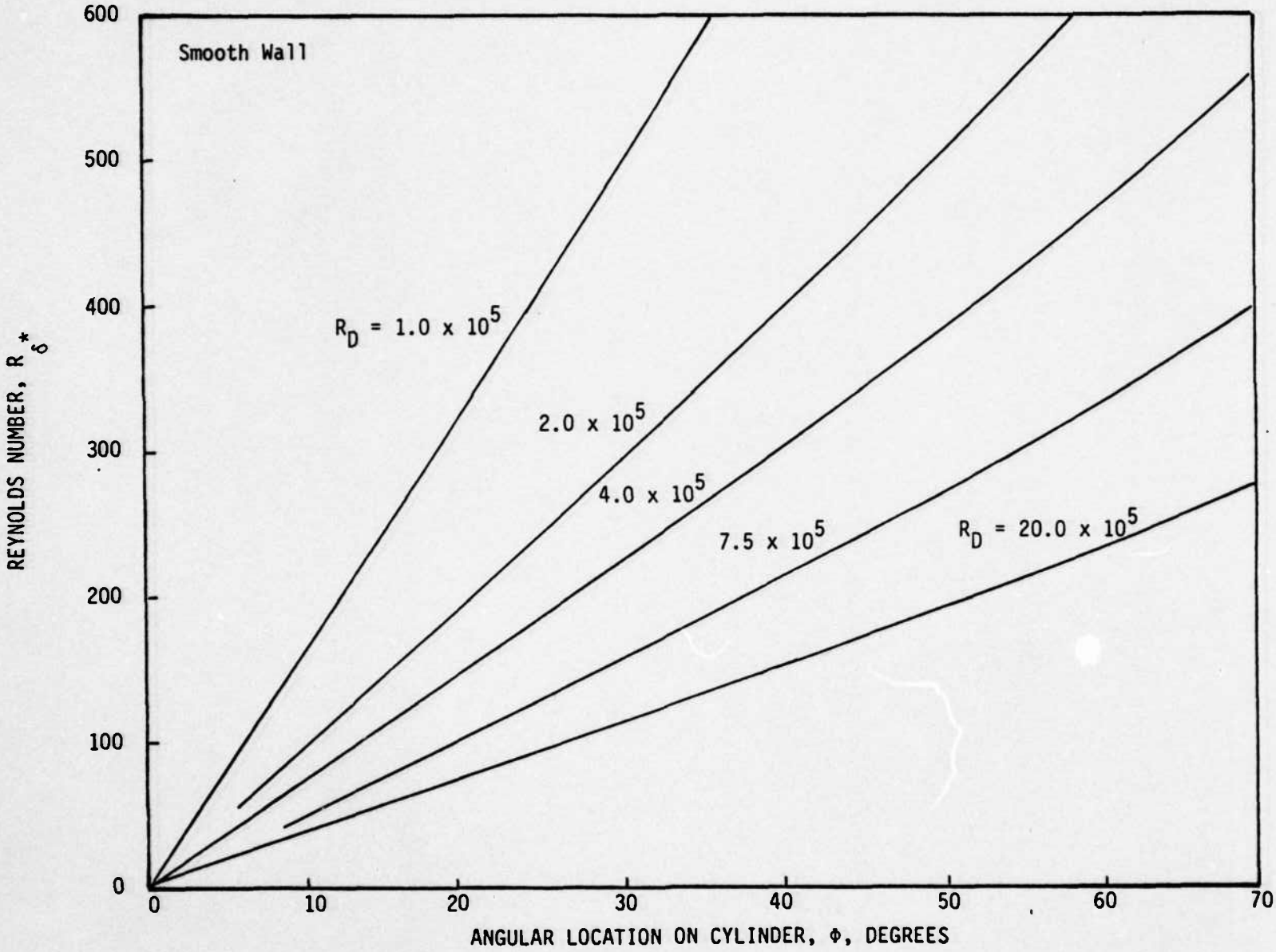

Figure 2. Boundary-Layer Reynolds Number on Smooth Wall Cylinder

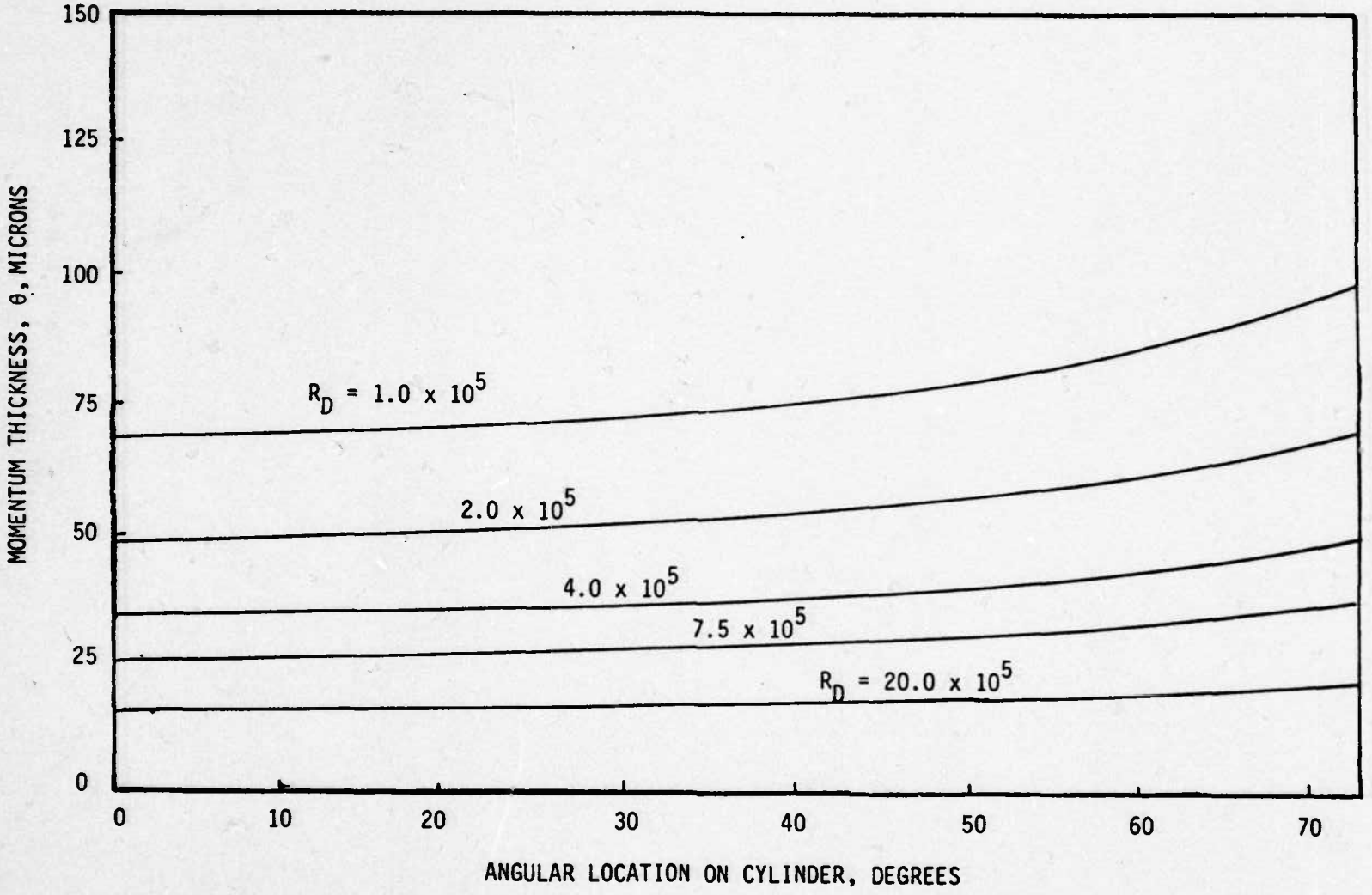

Figure 3. Smooth-Wall Momentum Thickness on Cylinder

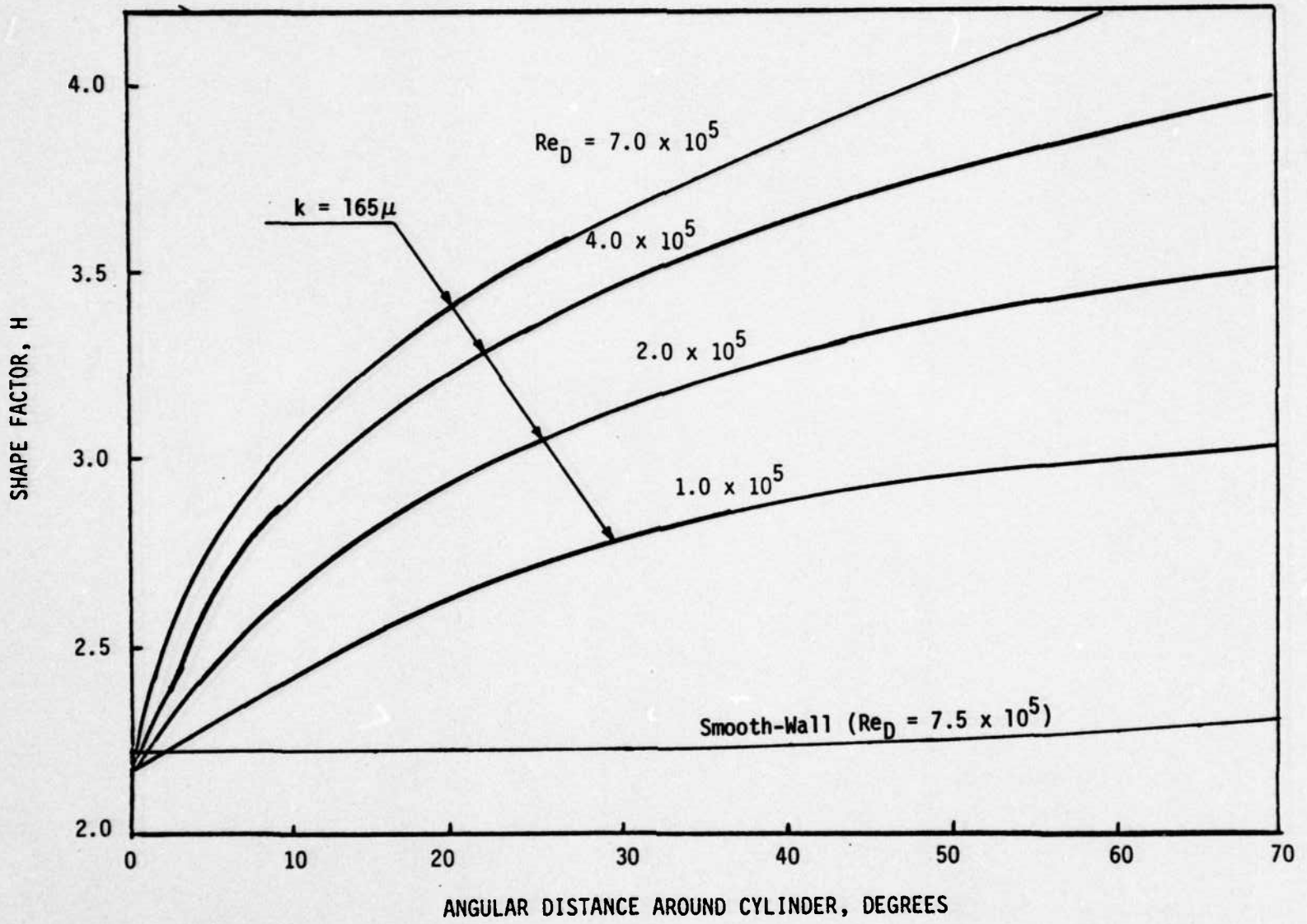

Figure 4. Boundary-Layer Shape Factor on Cylinder

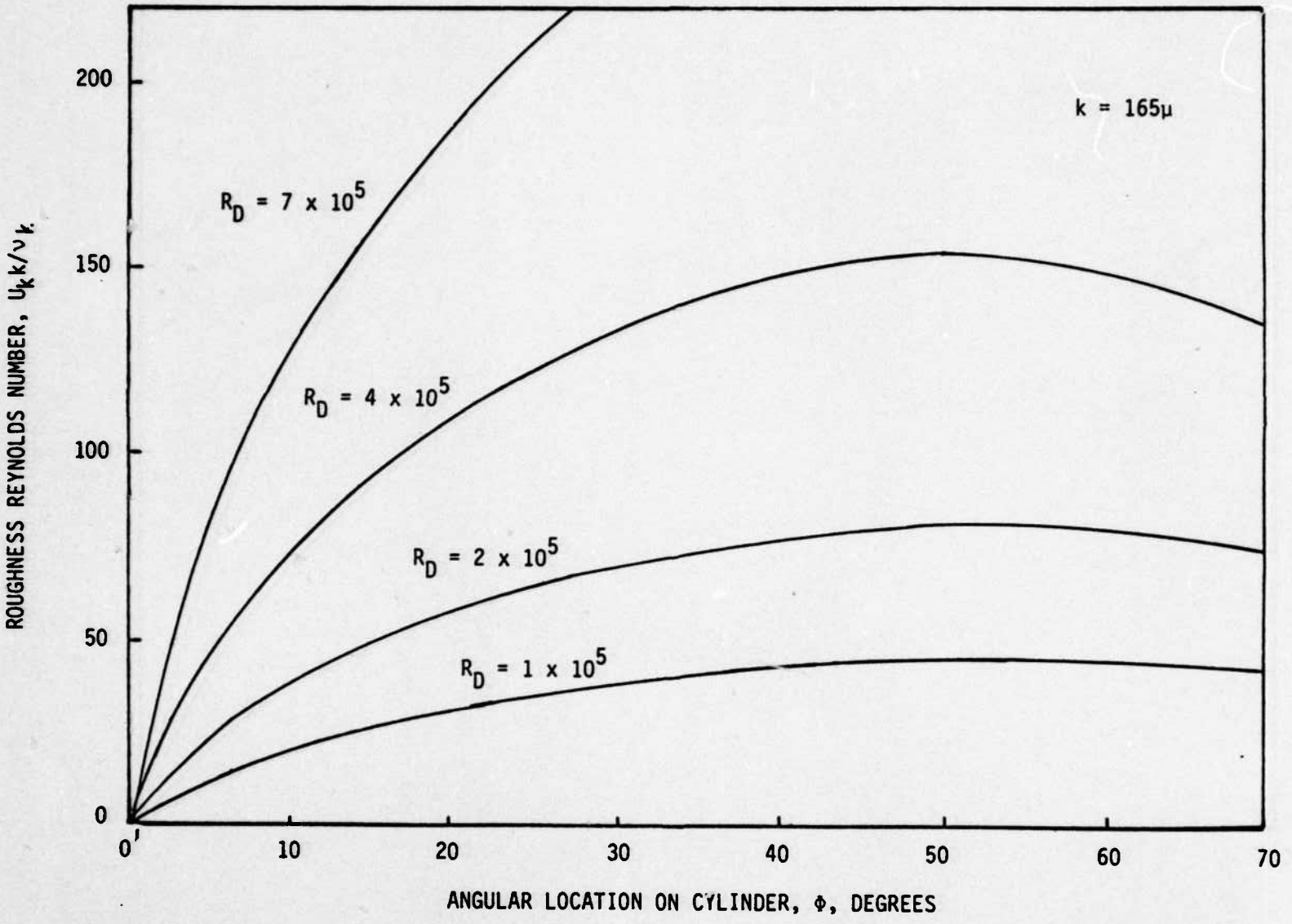

Figure 5. Roughness Reynolds Number on Cylinder

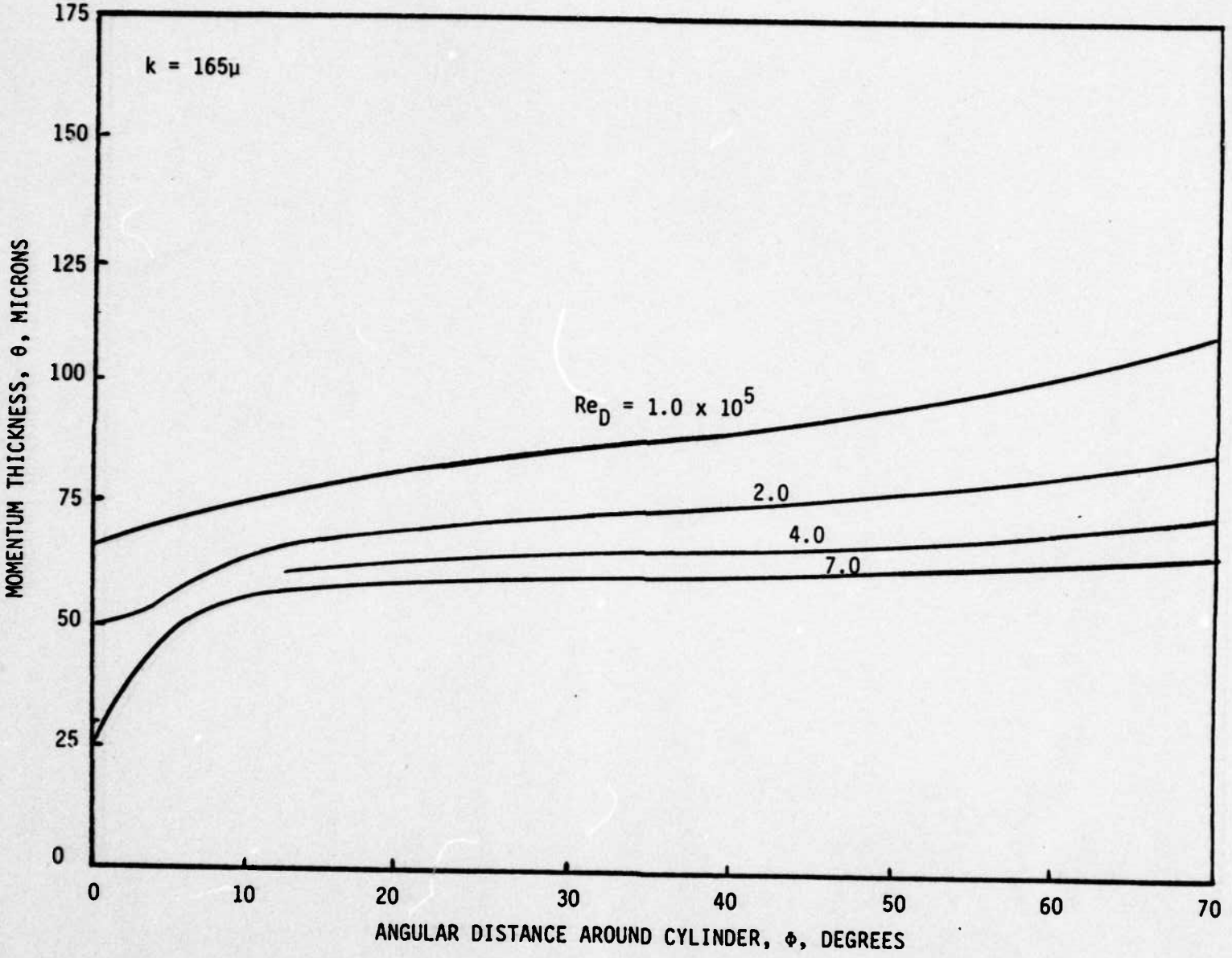

Figure 6. Momentum Thickness on Rough Cylinder

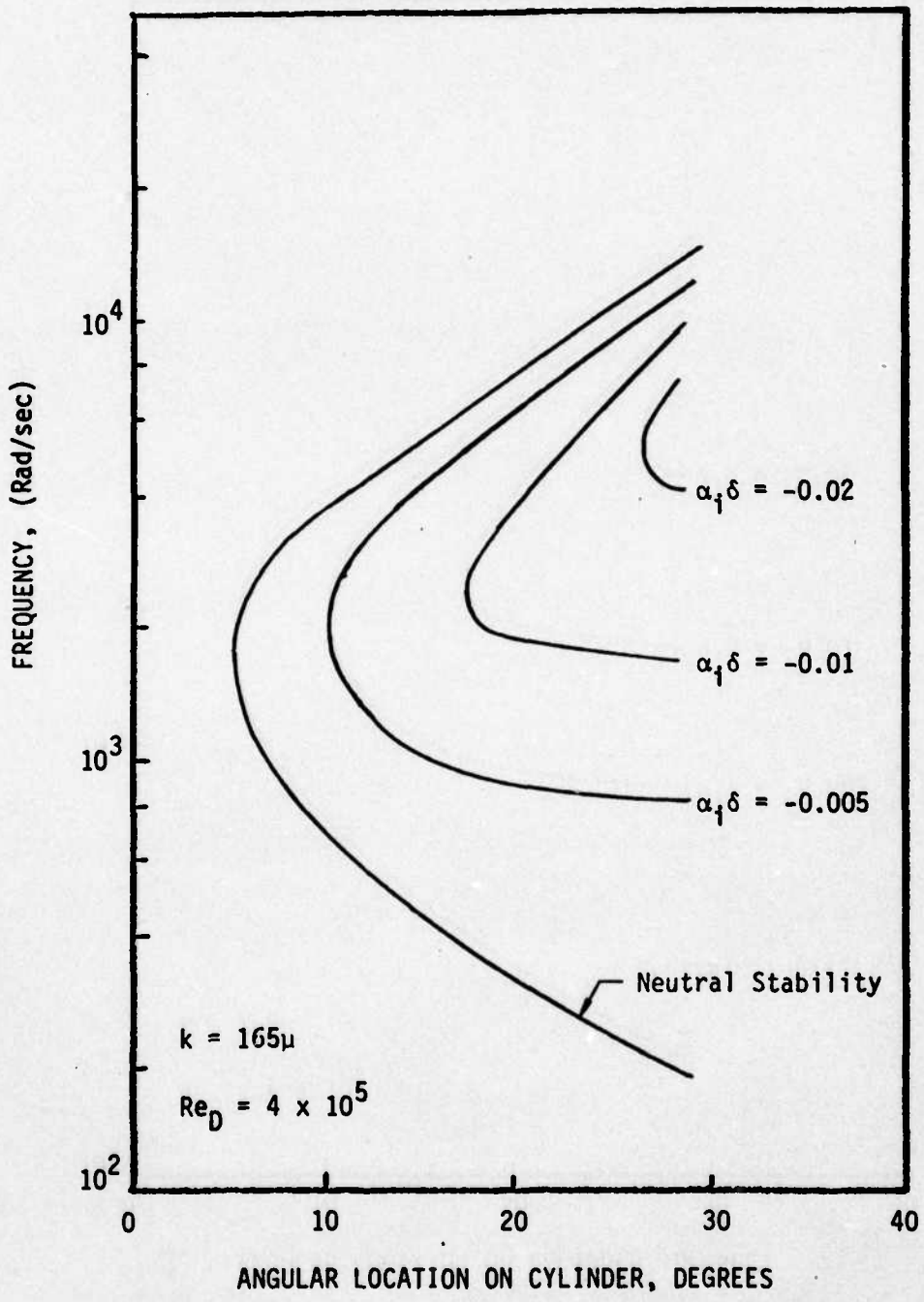

Figure 7. Stability Characteristics of Boundary Layer on Rough Cylinder

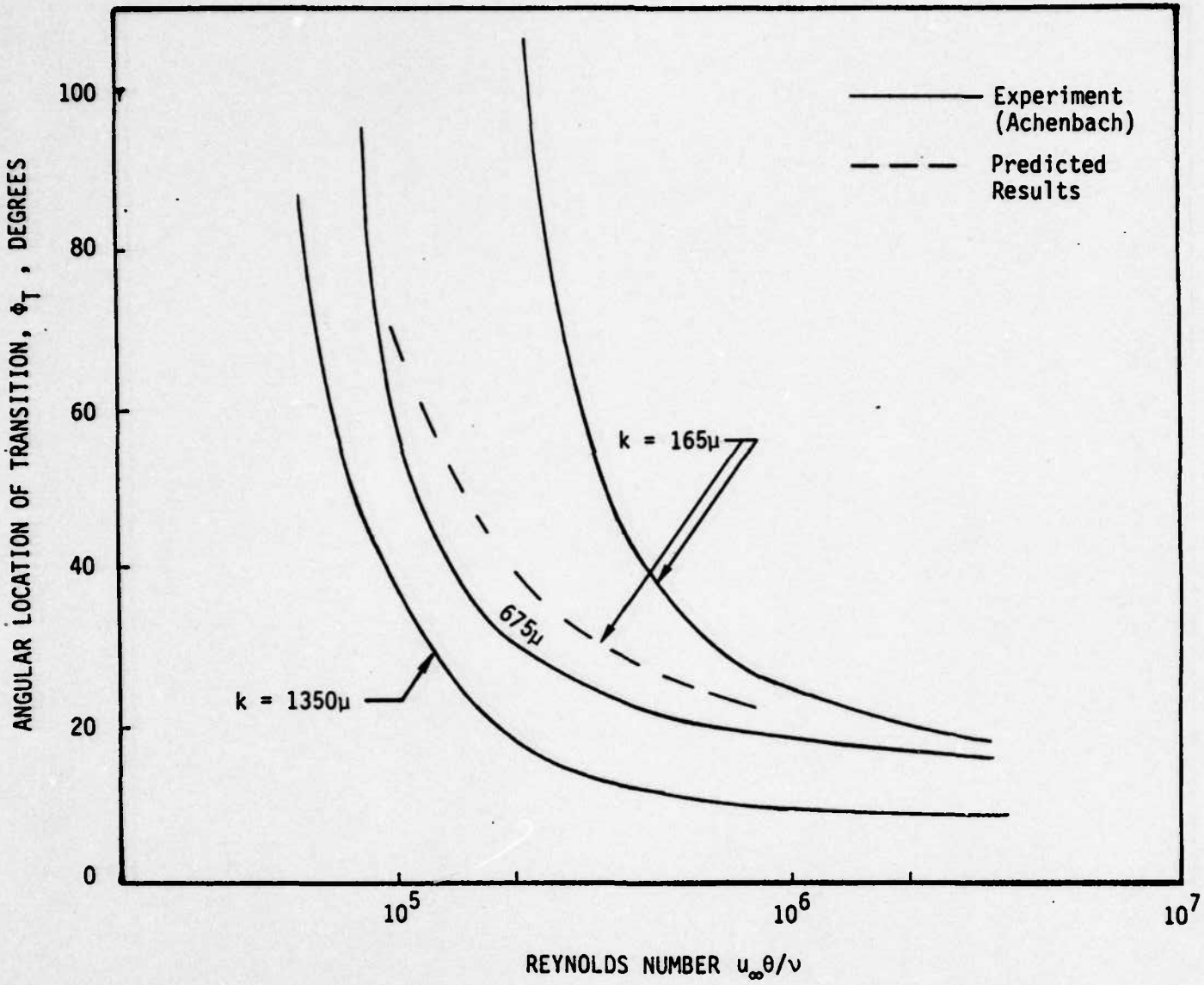

Figure 8. Transition Location on a Rough Cylinder

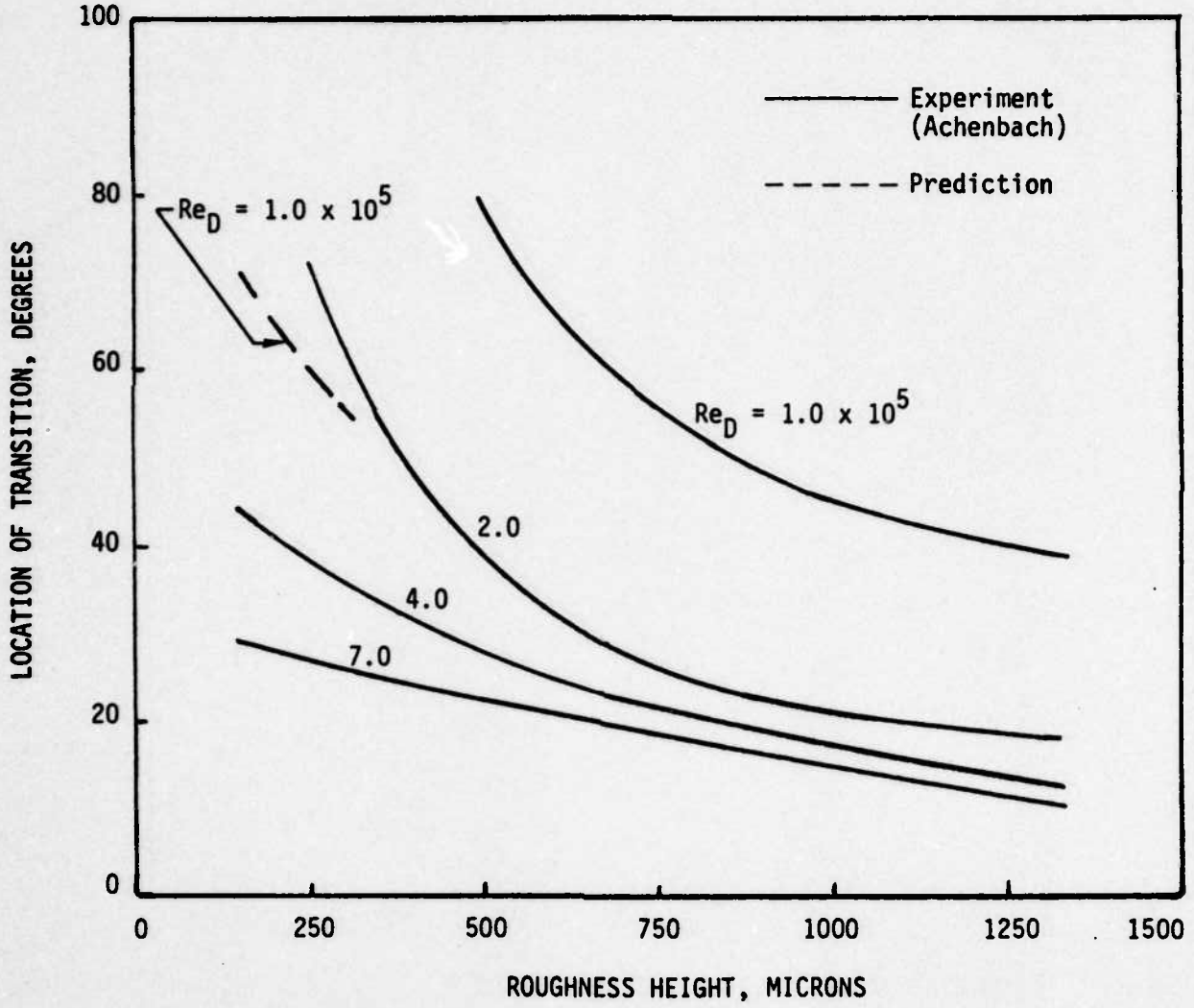

Figure 9. Effect of Roughness on Transition Location for a Cylinder

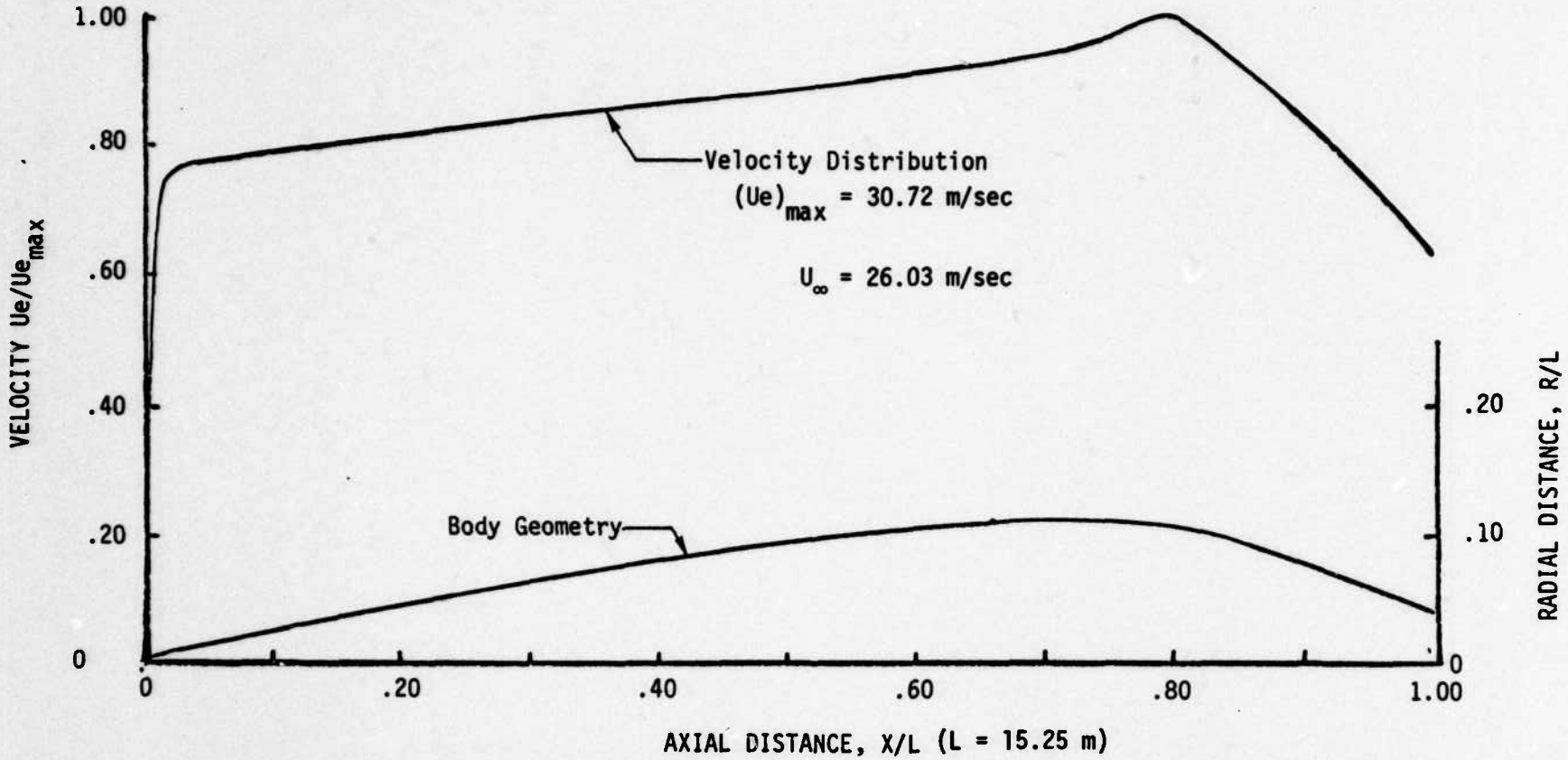

Figure 10. Geometry and Velocity Distribution for Body "H"

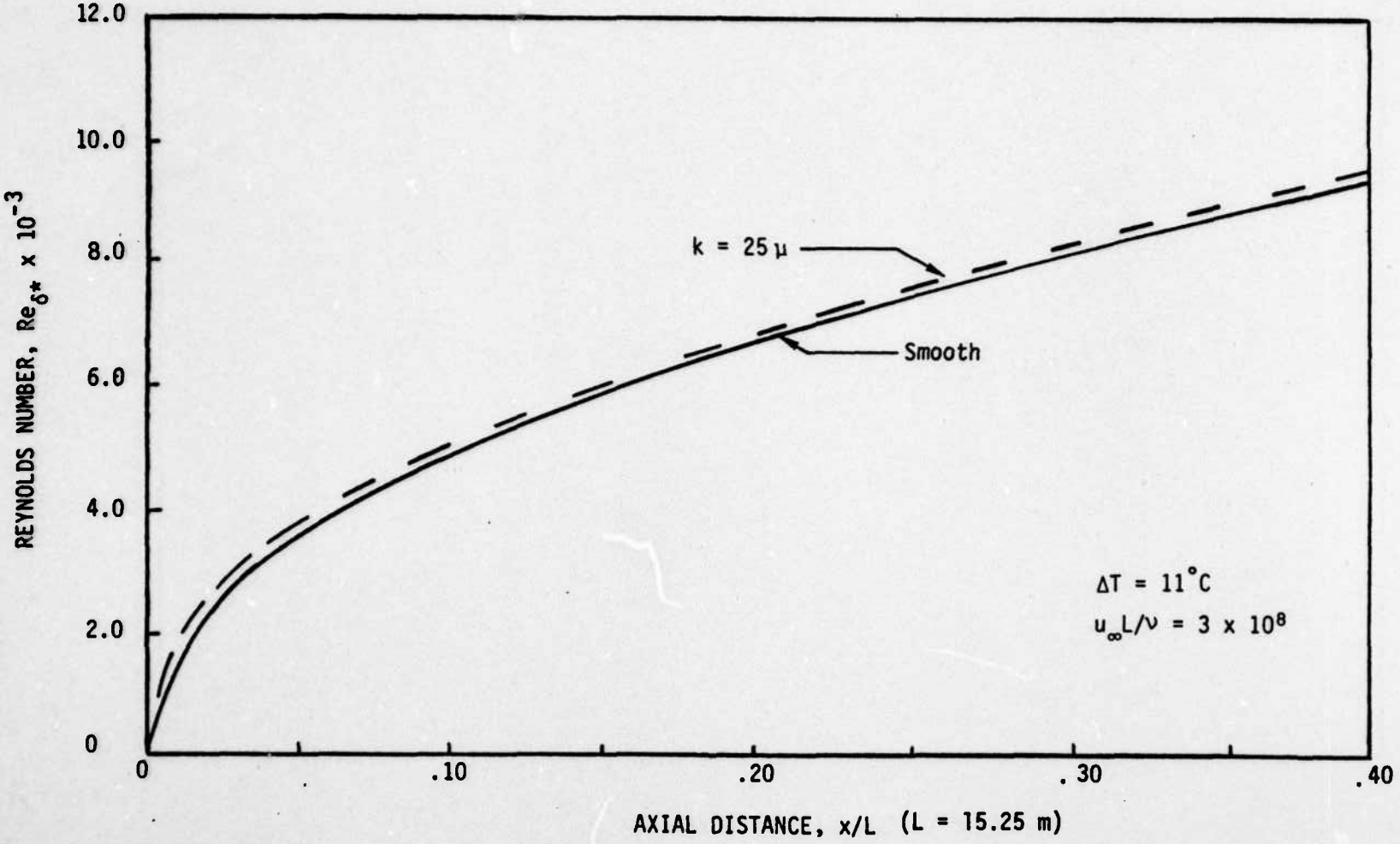

Figure 11. Effect of Roughness on Displacement Thickness Reynolds Number

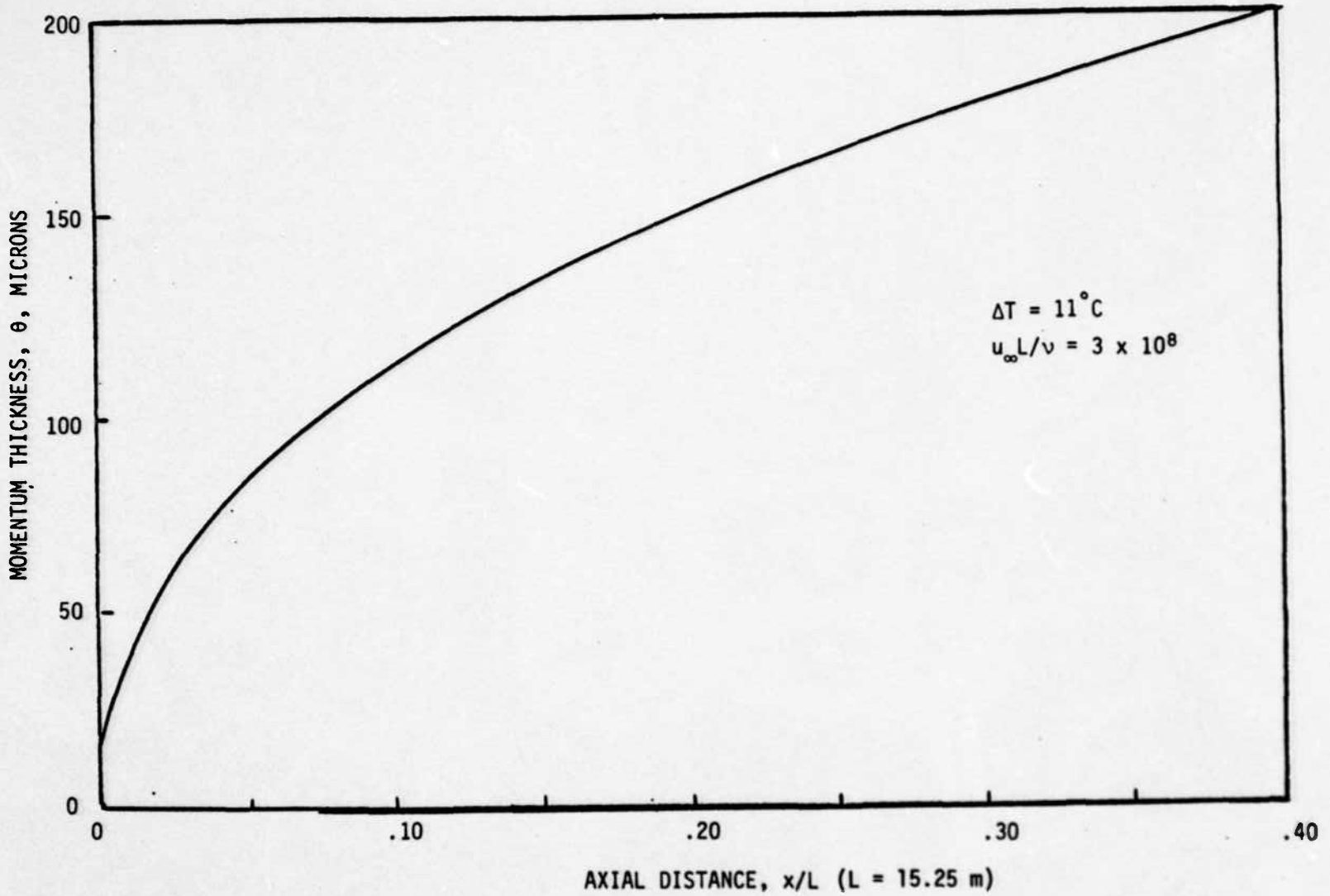

Figure 12. Variation of Momentum Thickness

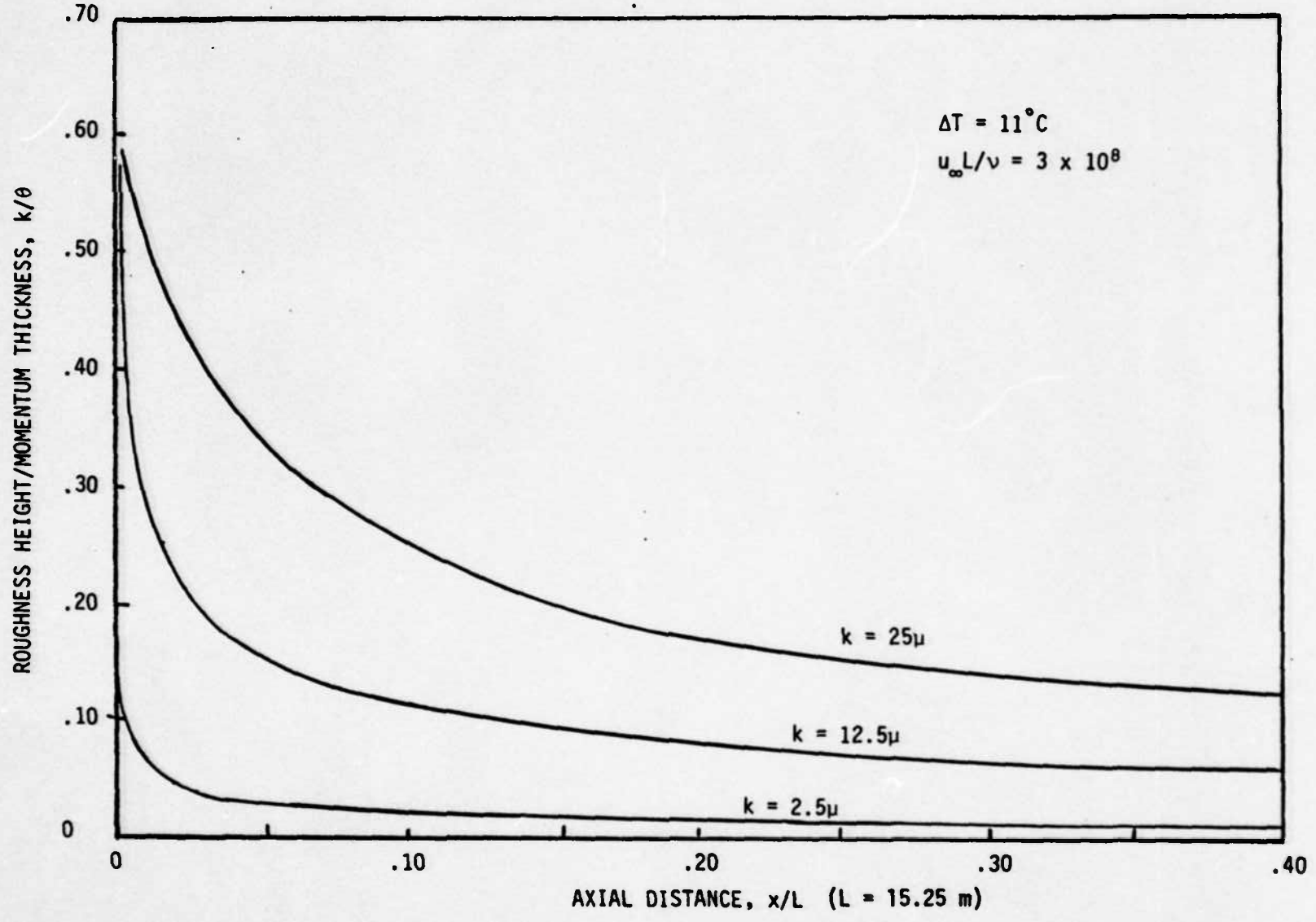

Figure 13. Variation of Roughness Height to Momentum Thickness Ratio

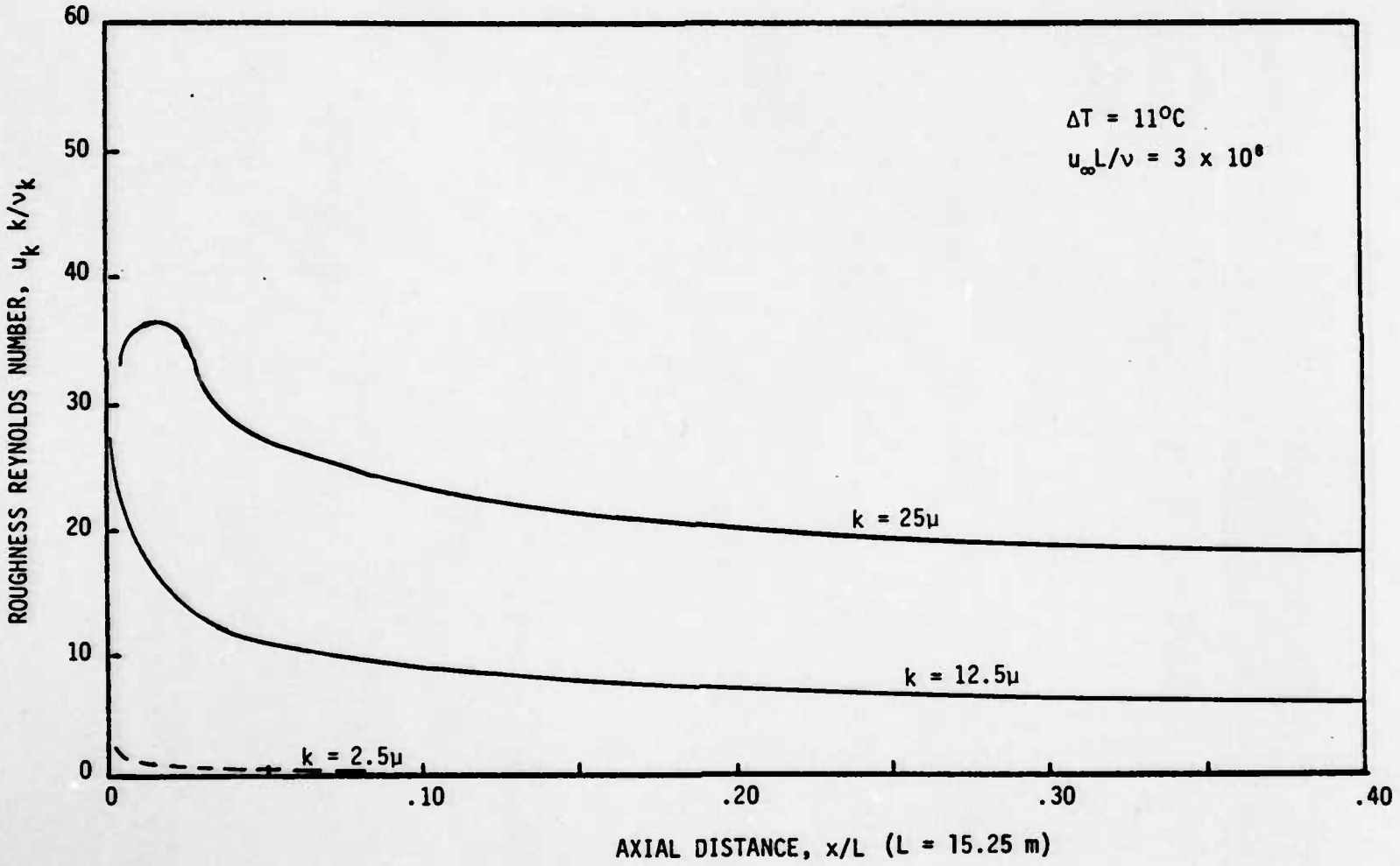

Figure 14. Variation of Roughness Reynolds Number

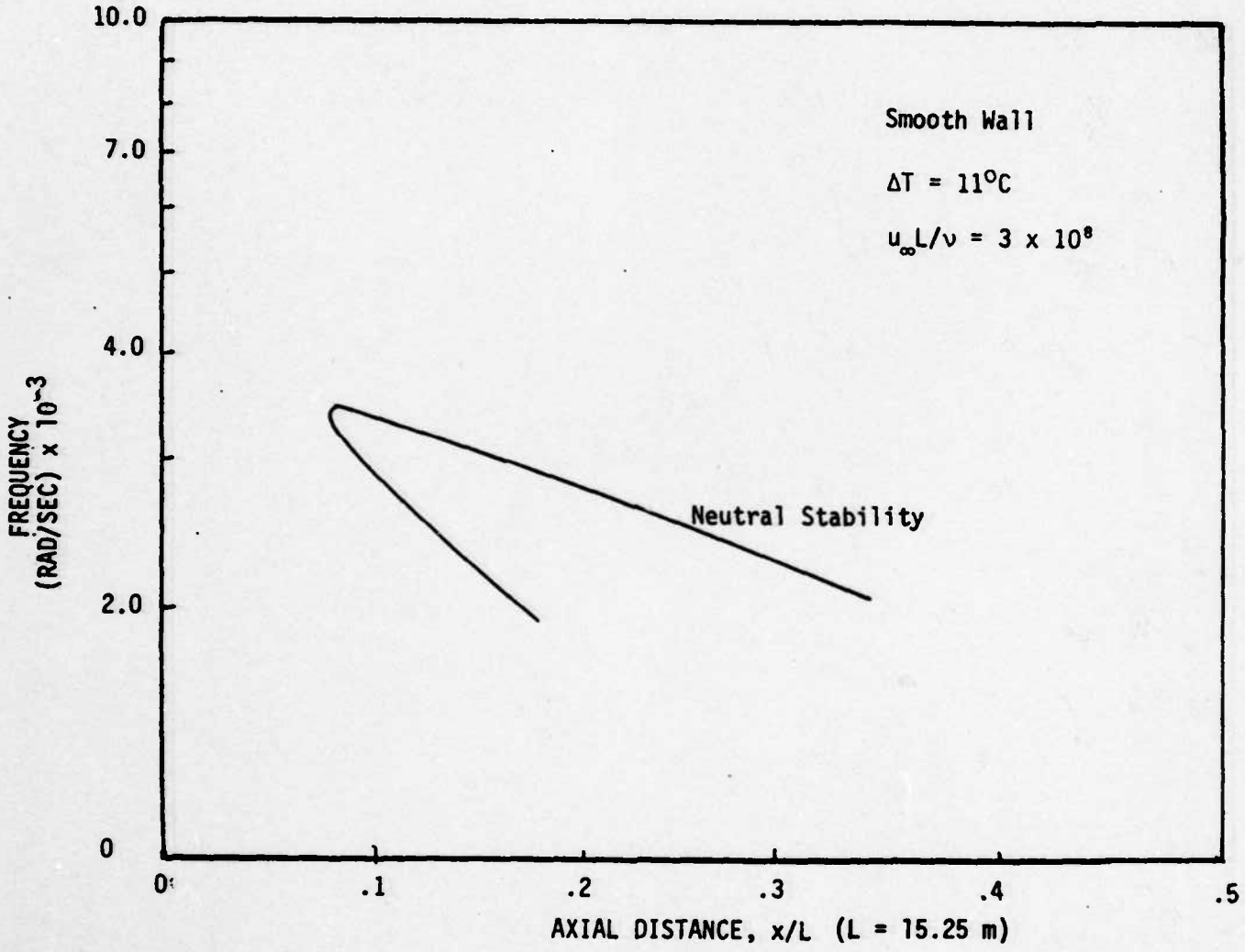

Figure 15. Stability Characteristics of Boundary-Layer on Smooth-Wall Body

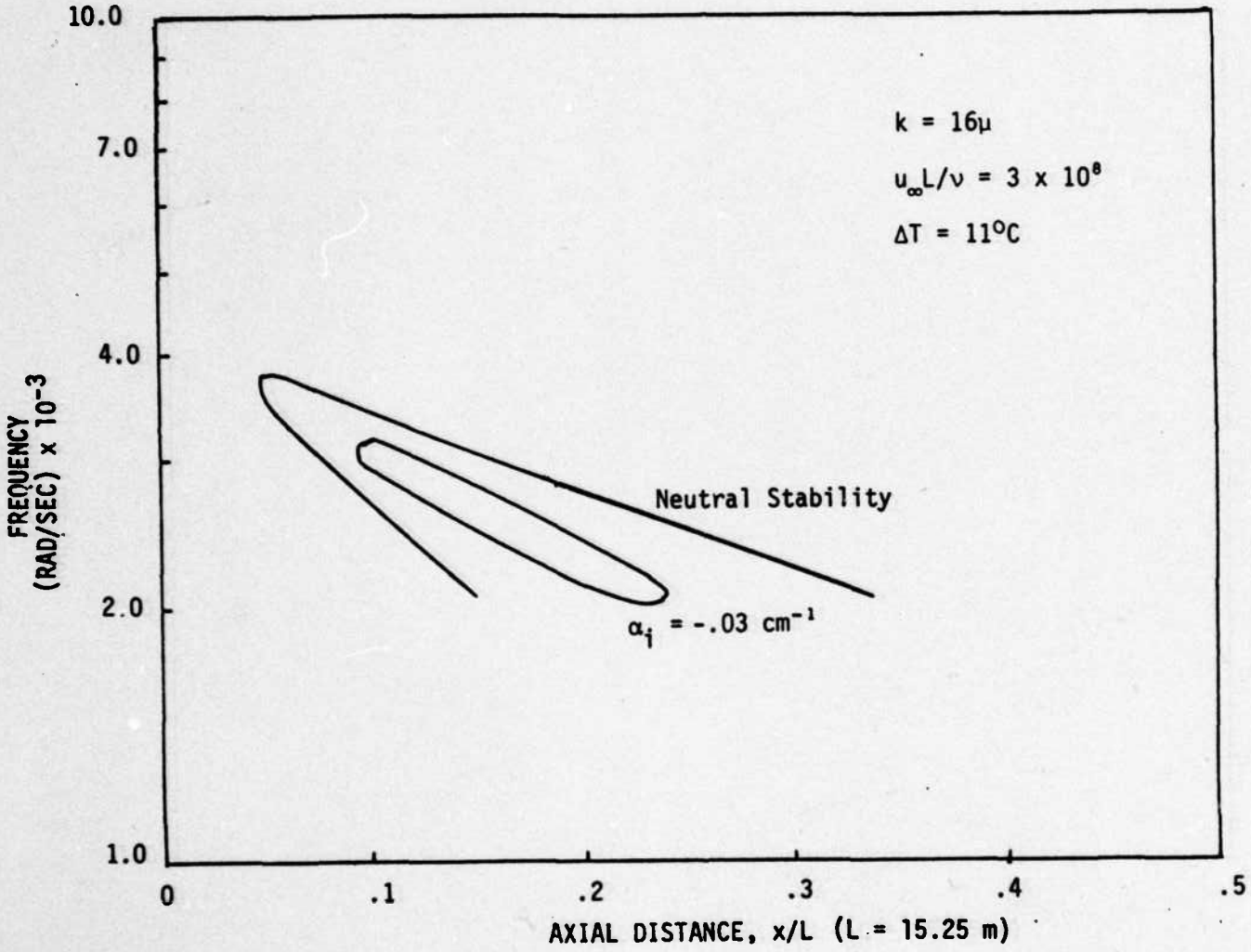

Figure 16. Stability Characteristics of Boundary-Layer on Heated Body with Rough Wall, k = 16μ

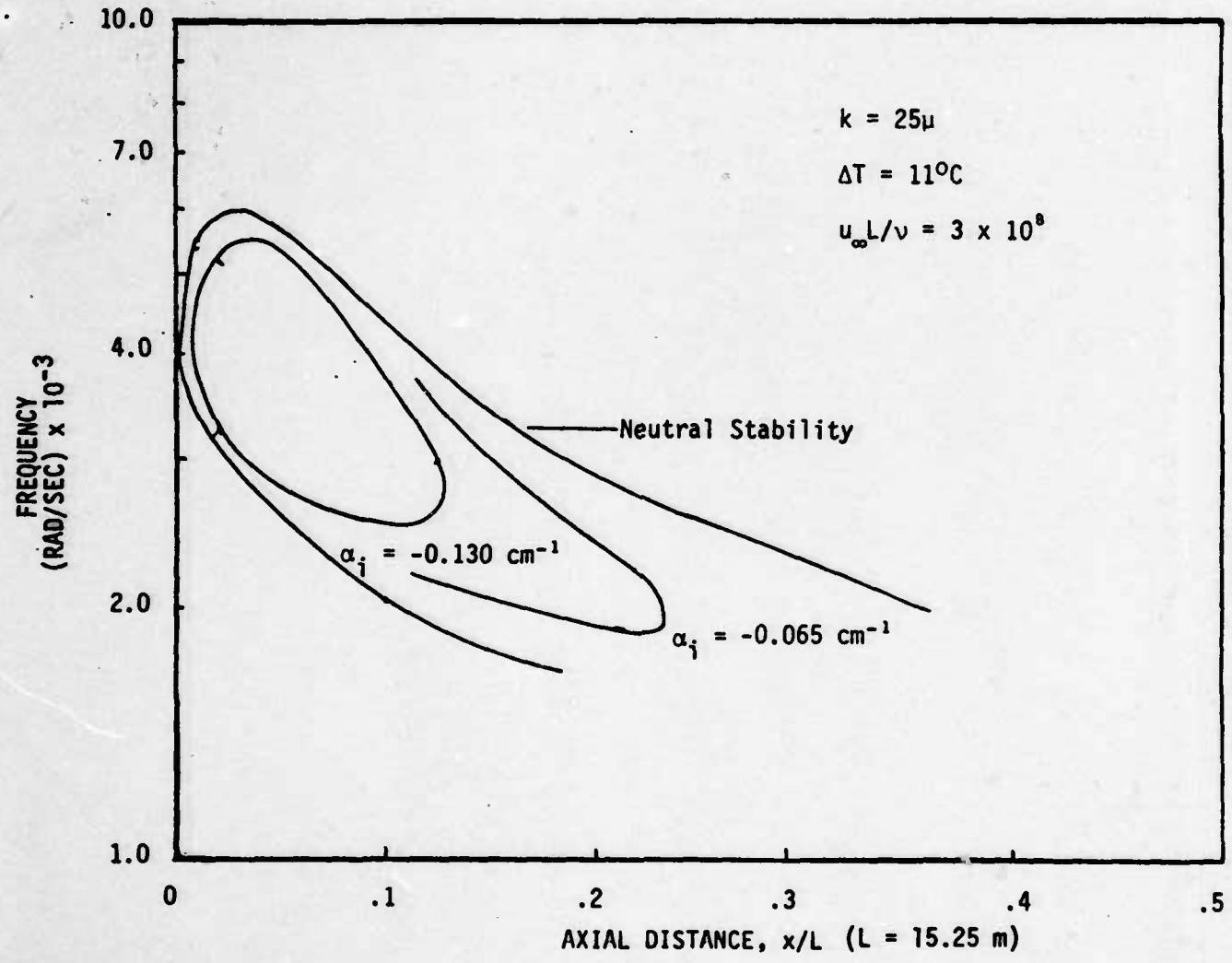

Figure 17. Stability Characteristics of Boundary-Layer on Heated Body with Rough Wall, k = 25μ

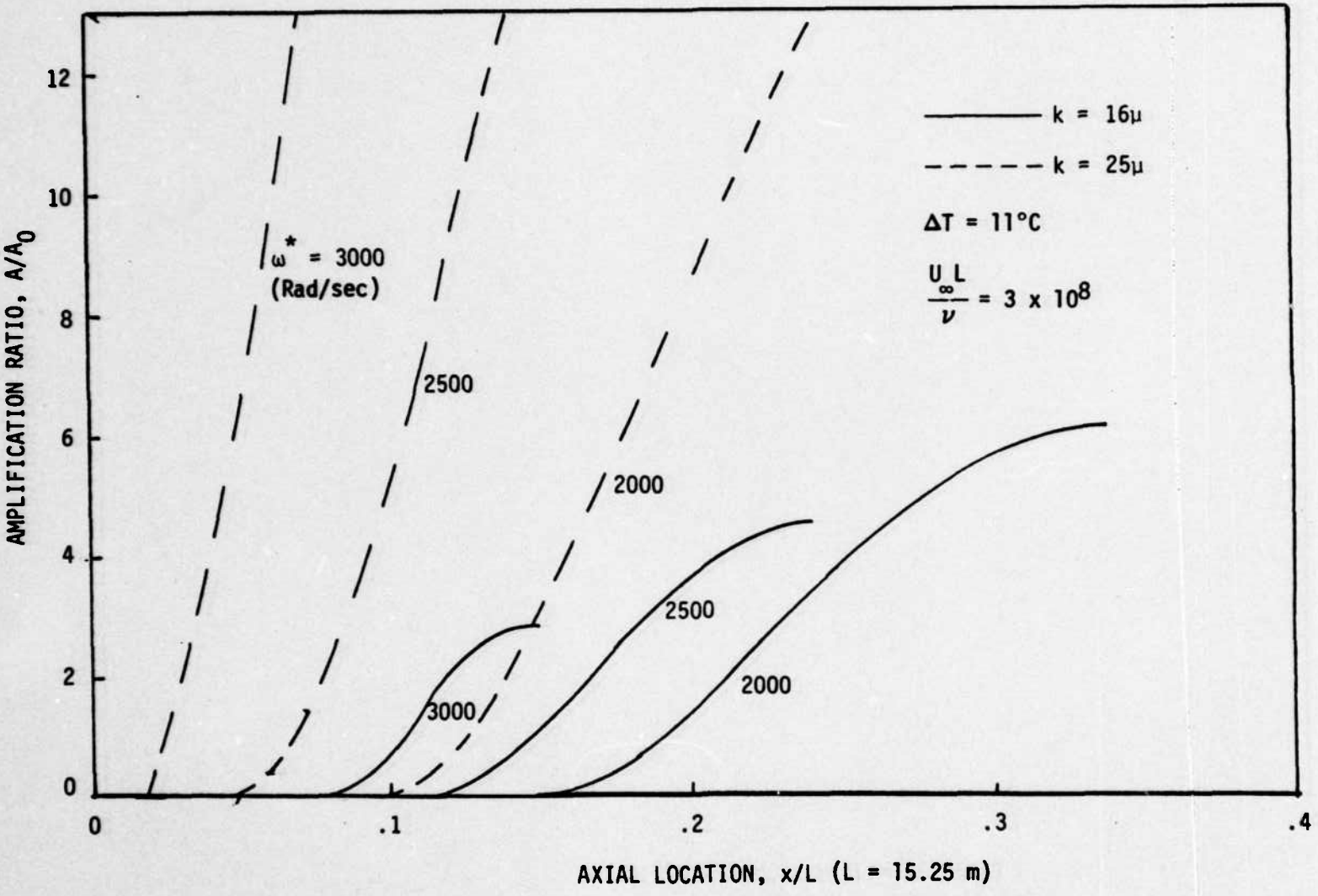

Figure 18. Disturbance Amplification Ratio Within Boundary Layer on Heated Body with Rough Wall

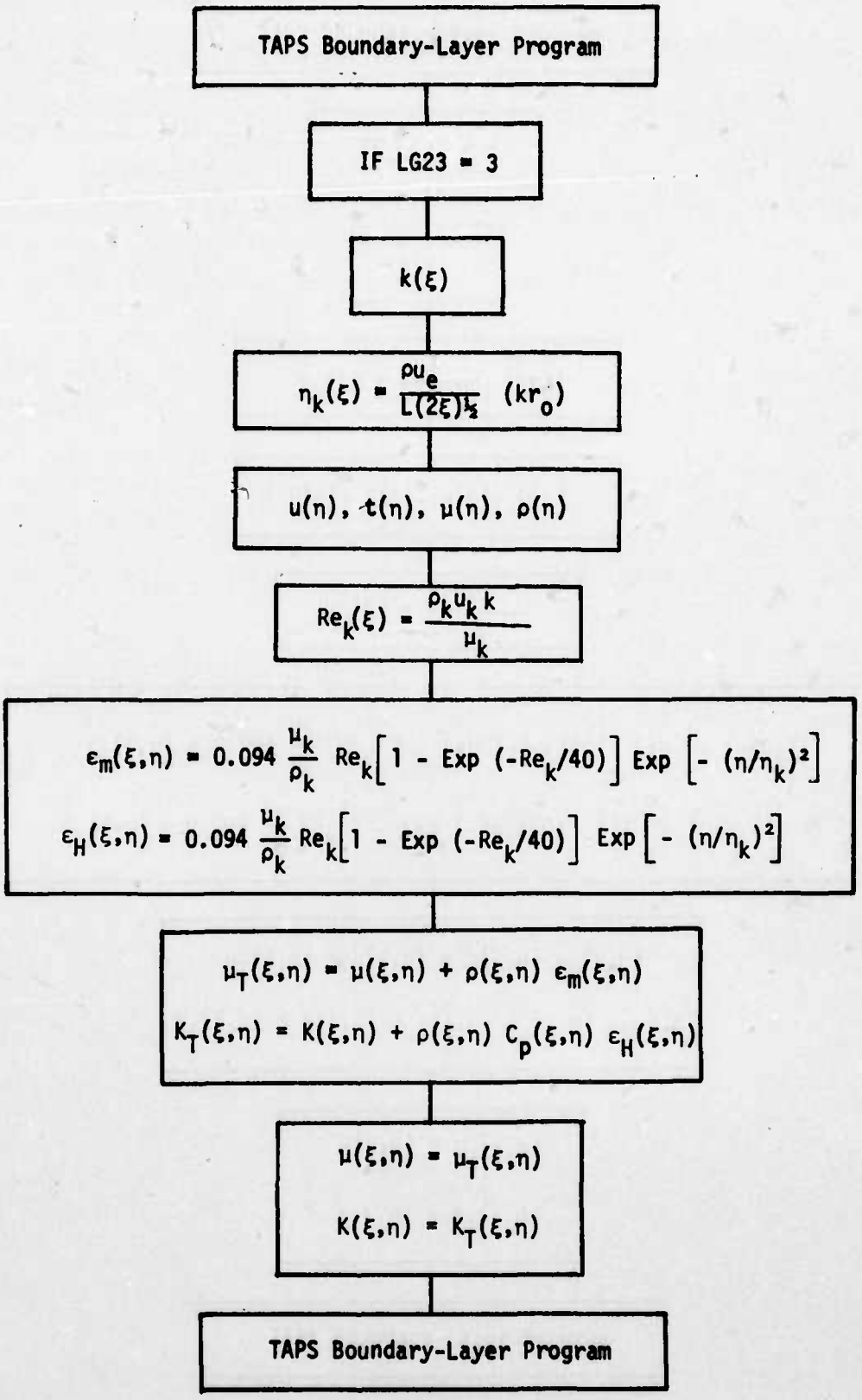

Figure 19. Flow Diagram for Incorporating Roughness Model into the TAPS Code

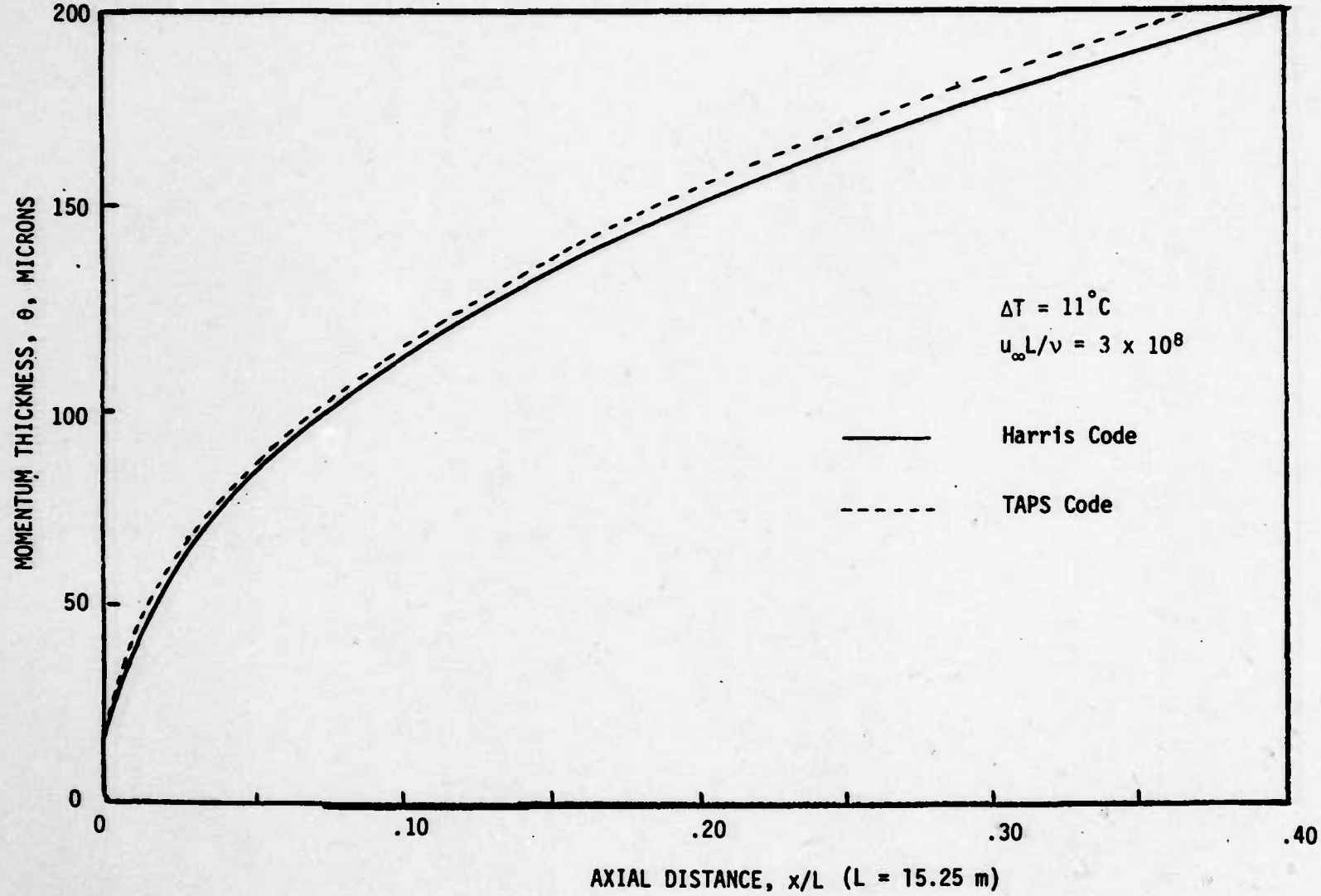

Figure 20. Comparison of Momentum Thickness

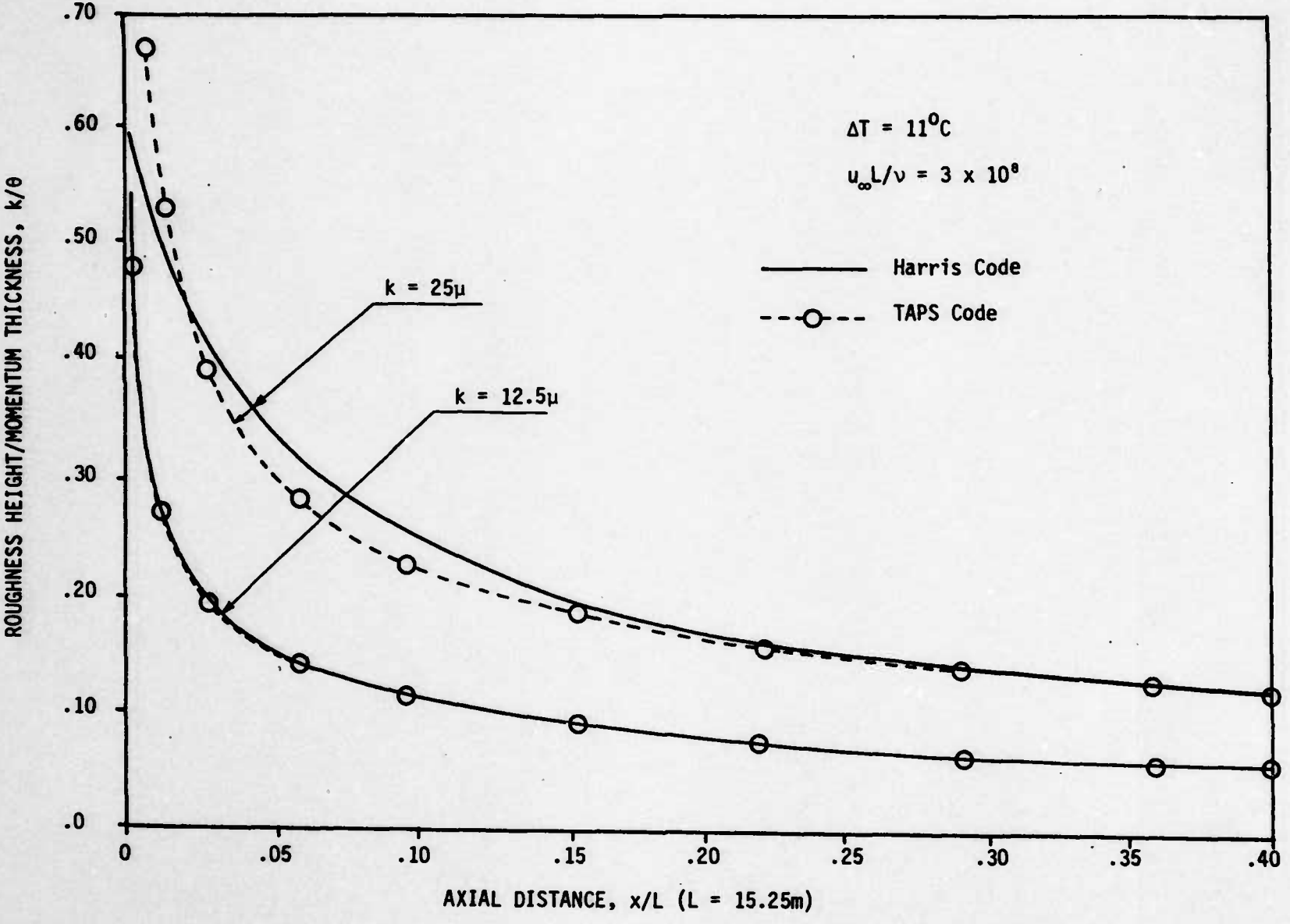

Figure 21. Comparison of Roughness Height to Momentum Thickness Ratio

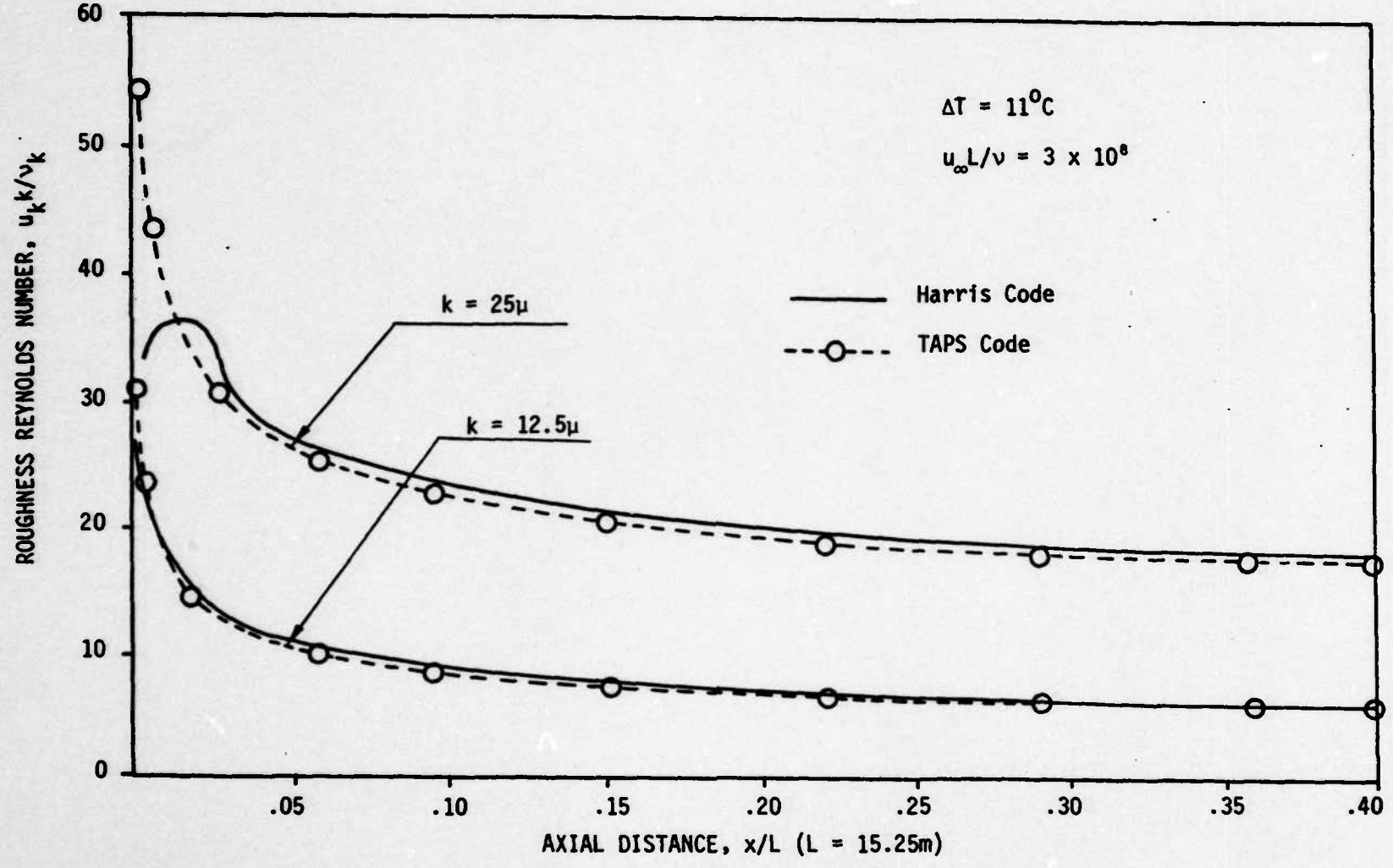

Figure 22. Comparison of Roughness Reynolds Number

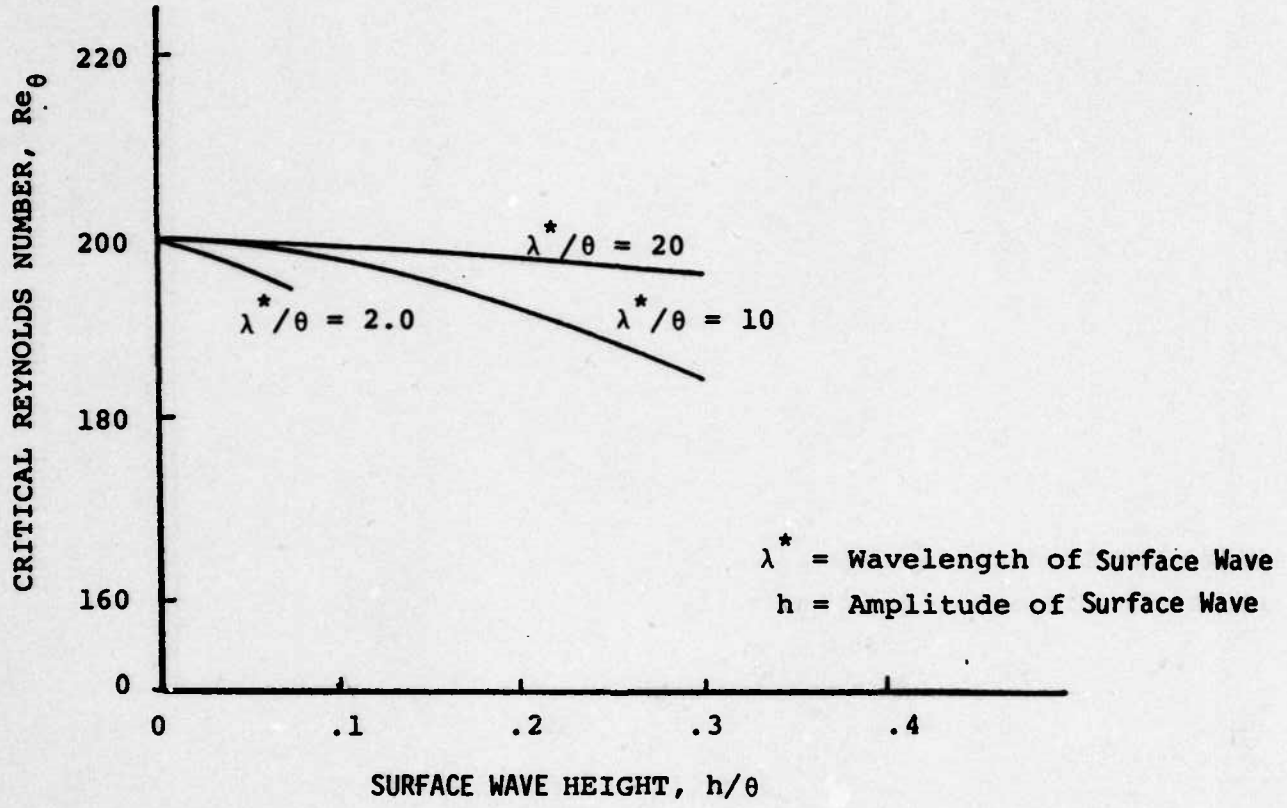

Figure 23. Effect of Wavy Wall on Critical Reynolds Number

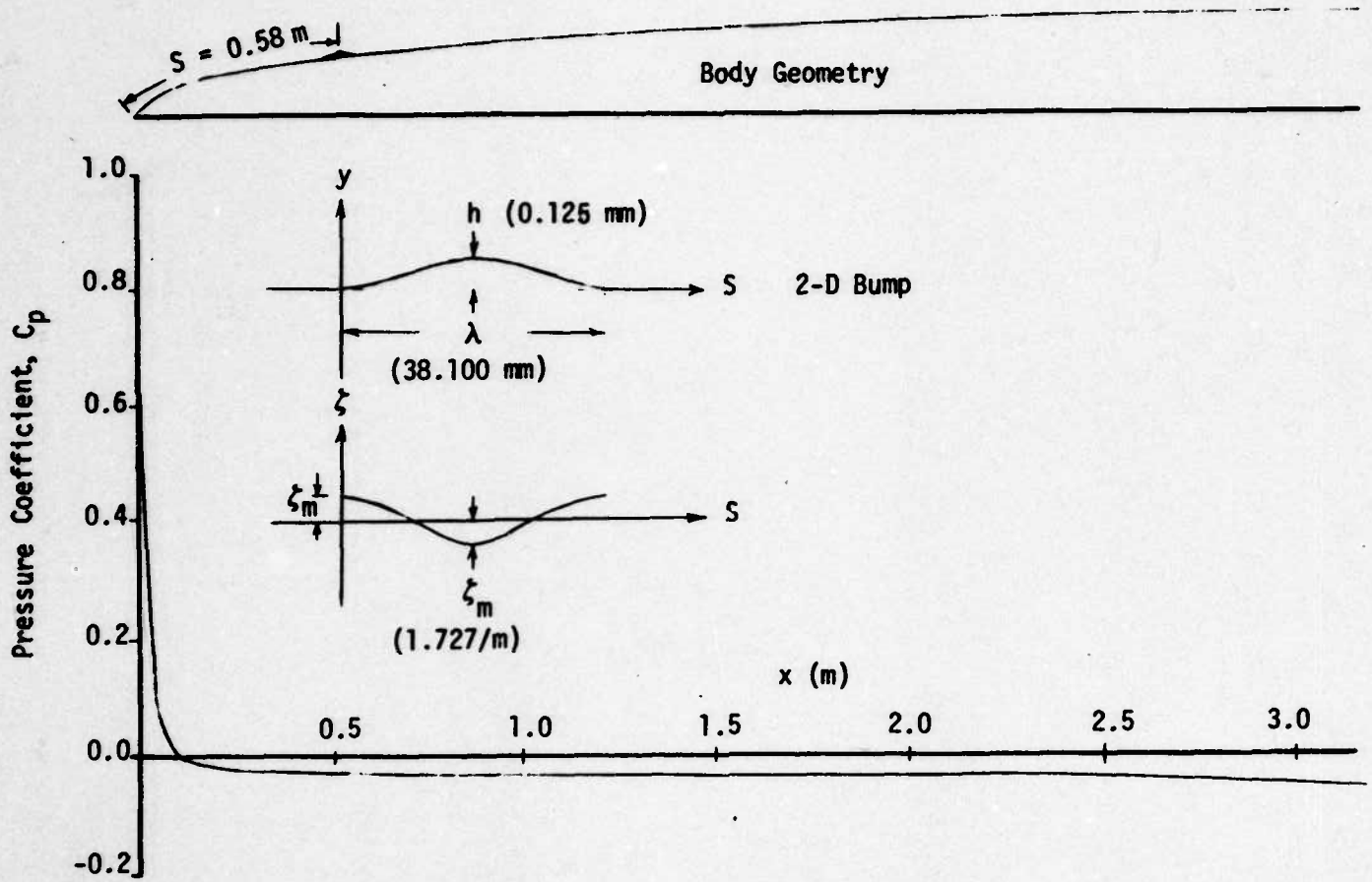

Figure 24. Geometry and Pressure Distribution for Reichardt Body

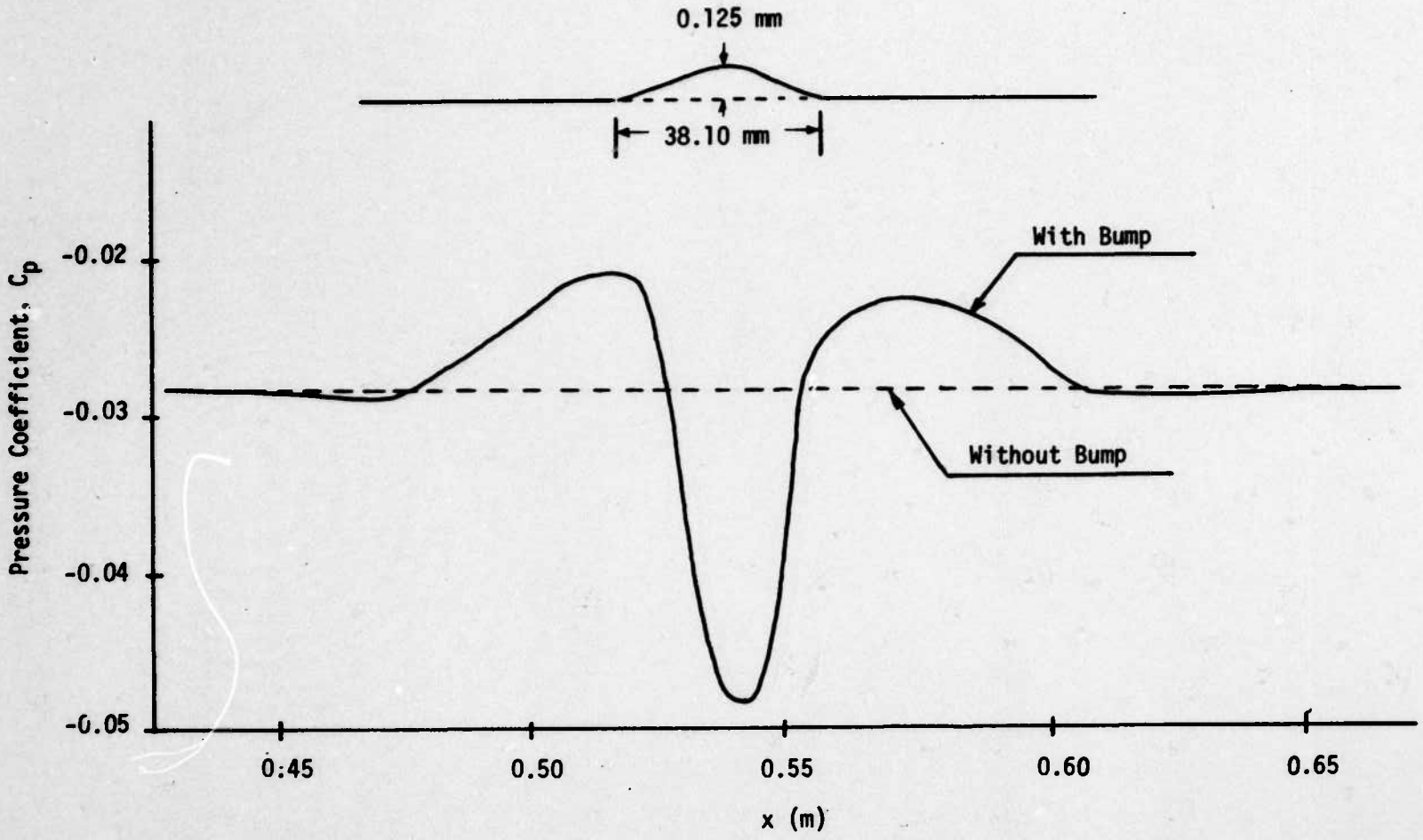

Figure 25. Effect of Single Bump on the Pressure Distribution

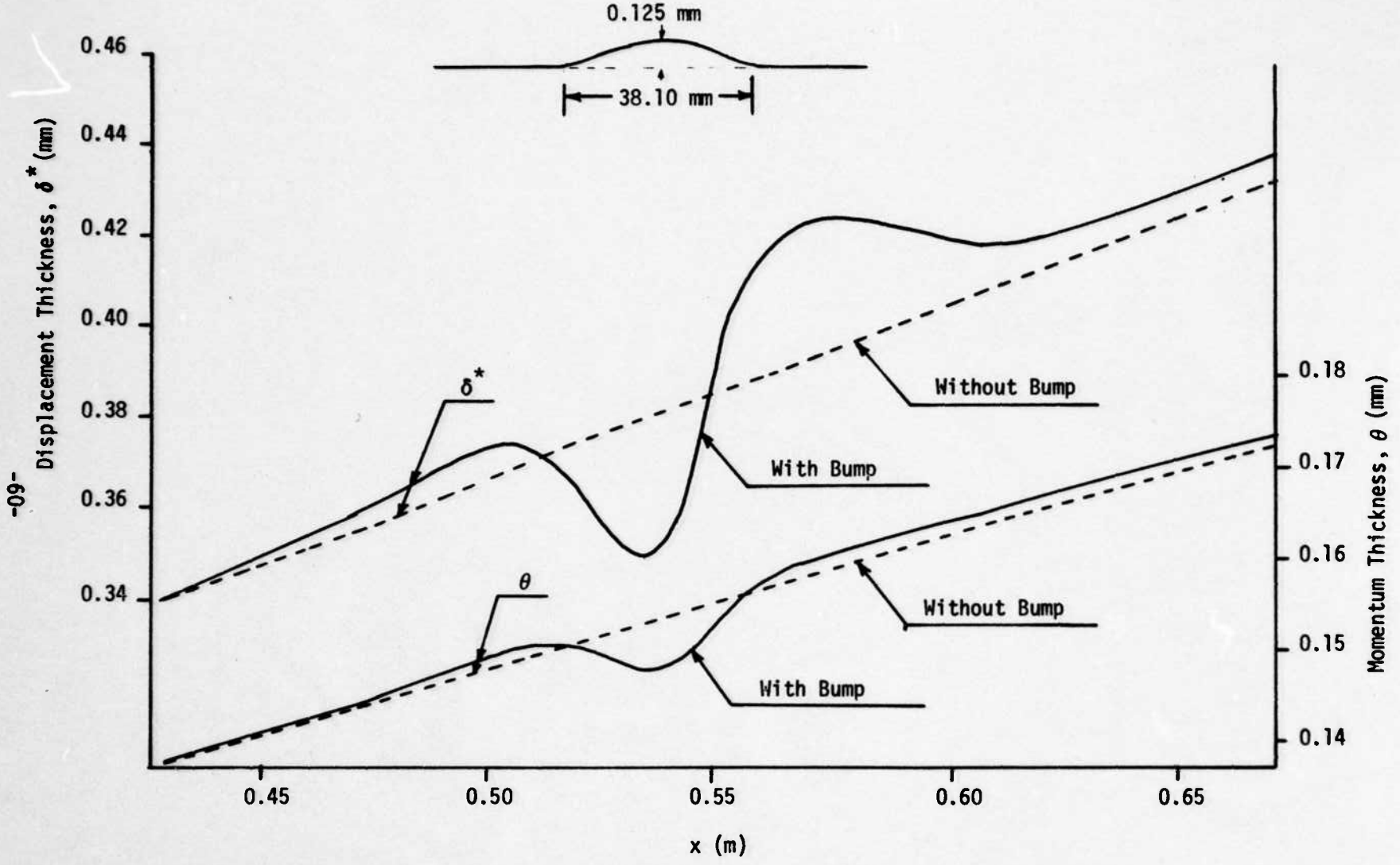

Figure 26. Effect of Single Bump on the Boundary-Layer Displacement Thickness and the Momentum Thickness

DISTRIBUTION LIST FOR UNCLASSIFIED
TECHNICAL REPORTS ISSUED UNDER
CONTRACT N00014-77-C-0005 TASK NR 062-562

All addressees receive one copy unless otherwise specified

Defense Documentation Center
Cameron Station
Alexandria, VA 22314 12 copies

Technical Library
David W. Taylor Naval Ship Research
and Development Center
Annapolis Laboratory
Annapolis, MD 21402

Library
Naval Academy
Annapolis, MD 21402

NASA Scientific and Technical
Information Facility
P.O. Box 8757
Baltimore/Washington Internat'l Airport
Maryland 21240

Librarian
Department of Naval Architecture
University of California
Berkeley, CA 94720

Professor P. Leehey
Department of Ocean Engineering
Massachusetts Institute of Technology
Cambridge, MA 02139

Dr. S. Orszag
Cambridge Hydrodynamics, Inc.
54 Baskin Road
Lexington, MA 02173

Library
Naval Weapons Center
China Lake, CA 93555

Professor E. Reshotko
Division of Chemical Engineering Science
Case Western Reserve University
Cleveland, OH 44106

Technical Library
Naval Surface Weapons Center
Dahlgren Laboratory
Dahlgren, VA 22418

Professor L. Landweber
Institute of Hydraulic Research
University of Iowa
Iowa City, IA 52242

Dr. D. R. S. Ko
Dynamics Technology, Inc.
3838 Carson Street, Suite 110
Torrance, CA 90503

Lorenz G. Straub Library
St. Anthony Falls Hydraulic Laboratory
University of Minnesota
Minneapolis, MN 55414

Library
Naval Postgraduate School
Monterey, CA 93940

Professor H. W. Liepmann
Graduate Aeronautical Laboratories
California Institute of Technology
Pasadena, CA 91109

Technical Library
Naval Ocean Systems Center
San Diego, CA 92132

Librarian
Naval Surface Weapons Center
White Oak Laboratory
Silver Spring, MD 20910

Fenton Kennedy Document Library
The Johns Hopkins University
Applied Physics Laboratory
Johns Hopkins Road
Laurel, MD 20810

Office of Naval Research
Code 438
800 N. Quincy Street
Arlington, VA 22217 3 copies

Office of Naval Research
Code 211
800 N. Quincy Street
Arlington, VA 22217

Office of Naval Research
Code 1021P (ONRL)
800 N. Quincy Street
Arlington, VA 22217 6 copies

Code 2627
Naval Research Laboratory
Washington, DC 20375 6 copies

Mr. T. Peirce (Code 03512)
Naval Sea Systems Command
Washington, DC 20362

Library (Code 09GS)
Naval Sea Systems Command
Washington, DC 20362

Library (Code 5641)
David W. Taylor Naval Ship Research
and Development Center
Bethesda, MD 20084

Mr. Dennis Bushnell
NASA Langley Research Center
Langley Station
Hampton, VA 23365

Dr. T. D. Taylor
The Aerospace Corporation
P.O. Box 92957
Los Angeles, CA 90009

Dr. Leslie M. Mack
Jet Propulsion Laboratory
California Institute of Technology
Pasadena, CA 91125

Dr. Phillip S. Klebanoff
National Bureau of Standards
Mechanics Division
Washington, DC 20234

Professor Tuncer Cebeci
California State University
Mechanical Engineering Department
Long Beach, CA 90840